

Linear-optical protocols for mitigating and suppressing noise in bosonic systems

Y. S. Teo,^{1,*} S. U. Shringarpure,^{1,*} S. Cho,¹ and H. Jeong^{1,†}

¹*NextQuantum and Department of Physics & Astronomy, Seoul National University, 08826 Seoul, South Korea*

Quantum-information processing and computation with bosonic qubits are corruptible by noise channels. Using interferometers and photon-subtraction gadgets (PSGs) accompanied by linear amplification and attenuation, we establish linear-optical methods to mitigate and suppress bosonic noise channels. We first show that by employing amplifying and attenuating PSGs respectively at the input and output of either a thermal or random-displacement channel, probabilistic error cancellation (PEC) can be carried out to mitigate errors in expectation-value estimation. We also derive optimal physical estimators that are properly constrained to improve the sampling accuracy of PEC. Next, we prove that a purely-dephasing channel is *coherently* suppressible using a multimode Mach–Zehnder interferometer and conditional vacuum measurements (VMZ). In the limit of infinitely-many ancillas, with nonvanishing success rates, VMZ using either Hadamard or two-design interferometers turns *any* dephasing channel into a phase-space-rotated linear-attenuation channel that can subsequently be inverted with (rotated) linear amplification *without* Kerr nonlinearity. Moreover, for weak central-Gaussian dephasing, the suppression fidelity increases monotonically with the number of ancillas and most optimally with Hadamard interferometers. We demonstrate the performance of these linear-optical mitigation and suppression schemes on common noise channels (and their compositions) and popular bosonic codes. While the theoretical formalism pertains to idling noise channels, we also provide numerical evidence supporting mitigation and suppression capabilities with respect to noise from universal gate operations.

I. INTRODUCTION

Advancement in our understanding of qubits encoded in continuous-variable (CV) bosonic modes (each governed by ladder operators $[a, a^\dagger] = 1$) [1–4] in terms of their generation and control [5–15] supplies ample evidence that these systems form vital resources in quantum-information processing [16–22] and computation [23–32]. In the current noisy intermediate-scale quantum (NISQ) era, unfortunately, such encoded CV systems are susceptible to bosonic noise channels [33–40]. Bosonic error correction [41–48] can potentially reduce logical error rates dramatically for sufficiently-small physical errors, ensuring reliable execution of quantum protocols running on bosonic qubits and that they possess distinct advantages from their *best-known* classical counterparts [49–58]. This, however, demands encodings corresponding to highly nonclassical states of (typically) multiple excitation modes, whose preparation remains a technological challenge.

With lower resource overheads, error-suppression methods employing specialized “cat” codes [59–61], noiseless attenuation and amplification [62–68] could reduce the impact of photon losses on bosonic systems. Techniques involving error filtration [69, 70] and virtual channel purification [71] were also proposed. By recognizing that observable expectation values are what is often sought after in a quantum task, error mitigation [72] also offers experimentally-feasible ways to further improve the quality of classical measurement outputs with postprocessing on symmetric bosonic codes [73, 74].

In this work, we introduce operationally feasible linear-optical protocols with classical postprocessing [75] to effectively mitigate and suppress common noise channels. Our methods do not rely on any specific bosonic encoding and can

also be demonstrated on platforms such as the superconducting architecture, wherein the equivalents of linear-optical elements are realized [76, 77]. Suppression of photon-loss channels using noiseless attenuation and amplification (noiseless loss suppression or NLS) on multicomponent “cat” codes was discussed in [68]. More recently, Ref. [78] proposed the use of probabilistic error cancellation (PEC) [79, 80] to invert the photon-loss channel.

We extend the aforementioned finding by employing *attenuating and amplifying photon-subtraction gadgets* (PSGs), comprising both linear-attenuation (or amplification) and photon subtraction operations, to mitigate general thermal (encompassing the familiar photon-loss channels) [81] and random-displacement noise (RDN) channels [82], a common type of which being Gaussian-displacement noise (GDN) channels [83, 84], which cannot otherwise be suppressed using NLS in general. We show that for arbitrary bosonic states and observables, these noise types can be asymptotically inverted by applying an *amplifying PSG before* and an *attenuating PSG after* the noise channel. As a way to circumvent the unphysical nature of amplifying PSGs that prevents any form of their deterministic implementation, we propose to carry out error mitigation using both PSGs and PEC on observable expectation values that permits the sampling of measurement outcomes constituting these amplifying PSGs as their indirect realization. As the expectation values are generally constrained, we develop optimal estimators that are properly constrained to maximize the PEC’s sampling accuracy.

Intuitively, when implemented indirectly through sampling, the first amplifying PSG map effectively spreads the encoded quantum information sufficiently far away from the phase-space origin, making space to introduce highly intensive interference reinforcements in order for the encoded qubit to sustain the effects of thermal noise or RDN. Thereafter, the second attenuating PSG undoes the spread and interference reinforcements to recover the encoded state.

Next, we discuss the *coherent error suppression* of bosonic

* These authors contributed equally to this work.

† h.jeong37@gmail.com

dephasing channels [37, 39, 85–90], which, for instance, models phase randomization in optical fibers under temperature and coherence fluctuation [91, 92] and quantum memories [93]. Such suppression attempts were previously known to be infeasible in practice as it requires nonlinear elements such as Kerr’s effect [78], with some recent progress on all-optical control of quantum states in exciton-polariton systems with coherent-triggering at single-photon levels and room temperatures [94]. In what shall be coined the *vacuum-based Mach–Zehnder* (VMZ) suppression scheme in this work, the input state immediately enters an input of a multimode interferometer before all output modes being subjected to independent and identically-distributed (i.i.d.) dephasing noise and another Hermitian-conjugated multimode interferometer afterwards. Finally, vacuum measurements on all output ancillas are performed. In the limit of infinitely-many ancillas, we found that VMZ with either Hadamard or unitary-two-design [95–98] interferometers turns any dephasing channel into a phase-space-rotated linear-attenuation channel with *nonvanishing* success probability, which may be subsequently inverted with linear amplification at the cost of a lower success rate. This presents a linear-optical dephasing-suppression protocol that requires neither feedforward nor nonlinear Kerr effects.

The working principle is that interference and interaction with dephasing results in VMZ functioning as an amplitude adder over all modes, which, for *any* dephasing distribution and large number of ancillary modes, leads to linear attenuation $\propto \lambda^{a^\dagger a} \rho_{\text{in}} \lambda^{*a^\dagger a}$ ($|\lambda| < 1$) on the noiseless input state ρ_{in} by virtue of the weak law of large numbers for certain common classes of interferometers. Furthermore, for a *finite number of ancillas* and weak dephasing rate, we show that for dephasing channels characterized by a central-Gaussian displacement distribution, the output-state fidelity after the VMZ scheme monotonically increases with the number of ancillas and is optimized by Hadamard interferometers.

We demonstrate the performance of error mitigation and suppression using the PSG and VMZ schemes (which are mutually commuting) for the common thermal, Gaussian-displacement and dephasing channels, as well as their combinations on well-established bosonic qubit encodings. We find that the output encoded-qubit fidelities improve significantly for reasonable noise rates, even in the presence of small measurement errors. Despite the fact that all theoretical arguments in Secs. II and III apply to idling noise during the storage or propagation of encoded states, Sec. IV also numerically showcases our protocols’ capabilities in treating noise from universal gate operations, thereby presenting feasible linear-optical recipes for bosonic error mitigation and suppression.

II. MITIGATING THERMAL NOISE AND RDN

A. Thermal-noise and RDN channels

We write the optical state $\rho = \int \frac{(d\alpha)}{\pi} |\alpha\rangle P(\alpha, \alpha^*) \langle \alpha|$ in terms of its Glauber–Sudarshan P function and coherent states $\{|\alpha\rangle \langle \alpha|\}$, where $(d\alpha)/\pi$ is the phase-space

volume measure. Then, structurally, the thermal and random-displacement noise (RDN) channels relate through the displacement-operator (D) mixture

$$\mathcal{E}[\rho] = \int \frac{(d\alpha)}{\pi} P(\alpha, \alpha^*) \int \frac{(d\beta)}{\pi} p(\beta, \beta^*) \times D(\nu\beta) |\mu\alpha\rangle \langle \mu\alpha| D(\nu\beta)^\dagger. \quad (1)$$

For a thermal noise channel $\mathcal{E} = \mathcal{E}_{\text{therm}}^{(\eta, \bar{n})}$ defined by the thermal photon number $\bar{n} \geq 0$ and noise rate $0 \leq \eta \leq 1$, $\nu = \sqrt{\eta} = \sqrt{1 - \mu^2}$ and $p(\beta, \beta^*) = e^{-|\beta|^2/\bar{n}}/(\bar{n})$. The special case $\bar{n} = 0$ corresponds to the (vacuum-)loss channel.

On the other hand, a general RDN channel corresponds to $\mu = 1 = \nu$ and some normalized probability distribution $p(\beta, \beta^*)$. For a special case of such a channel which we shall focus on, namely the Gaussian-displacement noise (GDN) channel, we have $p(\beta, \beta^*) = e^{-|\beta|^2/\sigma^2}/(\sigma^2)$ for some $\sigma > 0$ characterizing its strength. It can be shown that an application of the quantum-limited amplification operation on the thermal-noise channel results in the GDN channel [25], namely $\mathcal{E}_{\text{GDN}}^{(\sigma)}[\rho] = \mathcal{A}_{1/(1-\eta)} \circ \mathcal{E}_{\text{therm}}^{(\eta, \bar{n})}[\rho]$, where $\sigma^2 = \eta(1 + \bar{n})/(1 - \eta)$ and \mathcal{A}_G is the quantum-limited amplification map (details in Appendix A). The purpose of such a noise conversion (akin to Pauli twirling for discrete variables) was to facilitate the error correction of GDN using the Gottesmann–Kitaev–Preskill (GKP) code, although it is now known that this code may also correct thermal noise directly in conjunction with properly-optimized decoding methods [4]. Note also that $\mathcal{E}_{\text{GDN}}^{(\sigma')}[\rho] = \mathcal{E}_{\text{therm}}^{(\eta, \bar{n})}[\rho] \circ \mathcal{A}_{1/(1-\eta)}$, where $\sigma'^2 = \eta(1 + \bar{n}) < \sigma^2$. Hence, as a conservative choice for testing error-mitigation capabilities, we shall consider $\mathcal{E}_{\text{GDN}}^{(\sigma)}$, although for small η , both GDN channels are almost the same.

B. Asymptotic channel-inverting capability in PSGs

The amplifying or attenuating photon-subtraction gadget (PSG), characterized by a parameter $g > 0$, is a gadget consisting of either a noiseless linear amplifier ($g > 1$) or attenuator ($g < 1$), and photon subtraction. Its complete action may be described by the trace-preserving (TP) map

$$\mathcal{M}_{\text{PSG}, g}[\cdot] = \sum_{k=0}^{\infty} \frac{(-1 + g^{-2})^k}{k!} a^k g^{a^\dagger a} \cdot g^{a^\dagger a} a^{\dagger k} \quad (2)$$

for any g . *Only when* $g \leq 1$ is the map $\mathcal{M}_{\text{PSG}, g}$ completely positive (CP) and physically implementable in a deterministic way with photon counting after a beam splitter (BS) of transmittance g^2 .

Suppose that the quantum bosonic system traverses through an idling noise channel, which arises either during its storage or propagation, of the form in (1). Then, the channel-inverting scheme involves an amplifying PSG of gain factor $g > 1$ applied on the bosonic system before and another attenuating PSG of loss factor $g' < 1$ after the noise channel.

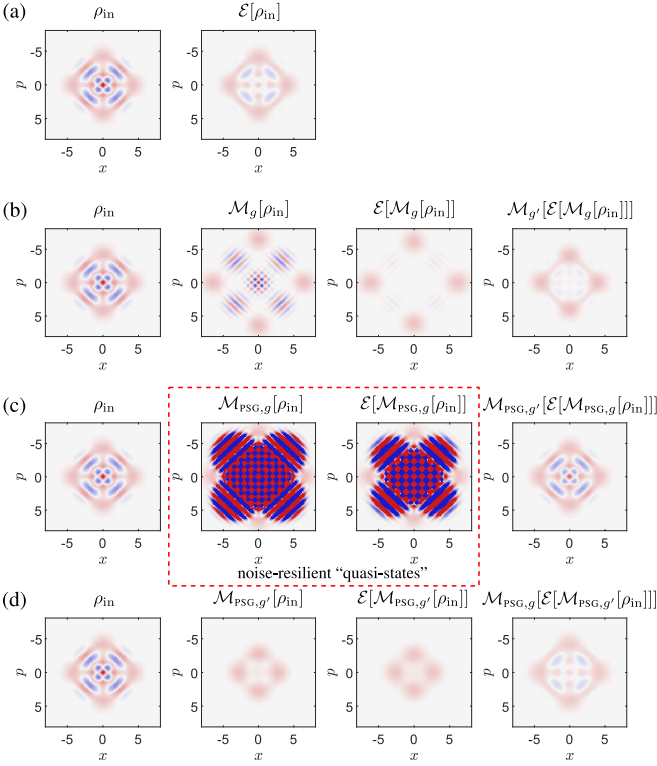


FIG. 1. A four-component “cat” state ($\propto |\alpha\rangle + |-\alpha\rangle + |i\alpha\rangle + |-i\alpha\rangle$) of amplitude $\alpha = 2$ undergoing (a) bare thermal-noise corruption ($\mathcal{F} = 0.475$), (b) through an ordered sequence of linear amplification, thermal noise and linear attenuation ($\mathcal{F} = 0.265$), and finally (c) through an ordered sequence of amplifying PSG, thermal noise and attenuating PSG ($\mathcal{F} = 0.825$). Here, $\eta = 0.1$ (a rate of 10%), $\bar{n} = 0.5$, $g = 1.6$ and $g' = 1/(1.6\sqrt{1-0.1}) = 0.659$. Although the Wigner functions in the two intermediate panels of (c) represent unphysical “quasi-states” due to the non-CP nature of amplifying PSGs, they nonetheless reveal the vital role photon subtraction plays as an amplitude modifier that protects interference features and nullify state distortion at the final output if such amplifying PSGs are realized through error mitigation (next subsection). The fortified Wigner-function interference is clearly seen in (c) and in striking contrast with (b), where the absence of photon subtraction leads to an almost completely washed-out Wigner interference fringes. (d) Note that reversing the PSG order results in an output state of very low quality ($\mathcal{F} = 0.424$).

Since

$$\mathcal{M}_{\text{PSG},g}[|\alpha\rangle\langle\alpha|] = |g\alpha\rangle\langle g\alpha|, \quad (3)$$

for any real g , when $g'\mu = 1$, the output state becomes

$$\begin{aligned} \rho_{\text{out}} &= \mathcal{M}_{\text{PSG},g'=1/(g\mu)<1}[\mathcal{E}[\mathcal{M}_{\text{PSG},g>1}[\rho_{\text{in}}]]] \\ &= \int \frac{(d\beta)}{\pi} p(\beta, \beta^*) D\left(\frac{\nu}{g\mu}\beta\right) \rho_{\text{in}} D\left(\frac{\nu}{g\mu}\beta\right)^\dagger, \quad (4) \end{aligned}$$

which is always a physical state since it is just a scaled RDN channel on ρ_{in} , despite the unphysical $\mathcal{M}_{\text{PSG},g>1}$. We then see that if $g \gg 1$, then $\rho_{\text{out}} \rightarrow \rho_{\text{in}}$ and noise-channel inversion is *asymptotically* achieved. A useful rule-of-thumb guide for

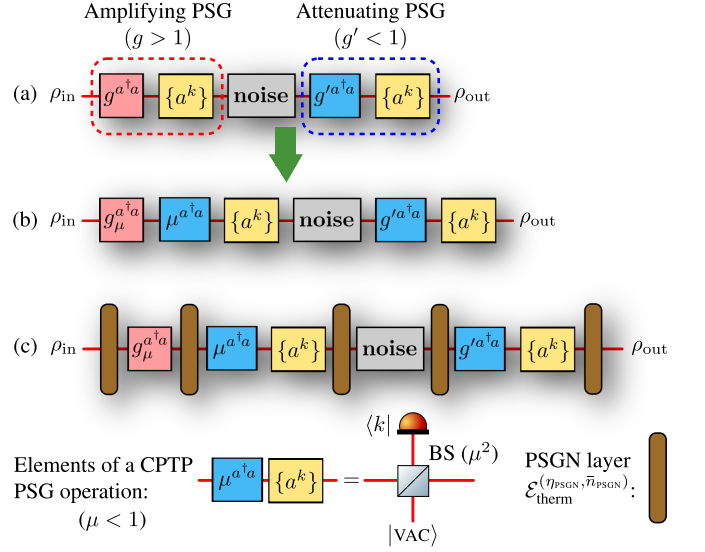


FIG. 2. The PSG-PEC mitigation setup. (a) The first amplifying PSG of a gain factor $g > 0$ is not CP and so cannot be directly realized. (b) One may portion it into a probabilistic amplification of gain $g_\mu = g/\mu$ and an attenuating PSG of parameter $0 < \mu < 1$. The choice of μ should optimize the error-mitigation performance. (c) More realistically, each distinct operation of the setup is noisy and may be accompanied by a PSGN layer before and another after the operation. The first PSGN layer may also account for ρ_{in} -preparation errors. We model each PSGN layer as a thermal channel $\mathcal{E}_{\text{therm}}^{(\eta_{\text{PSGN}}, \bar{n}_{\text{PSGN}})}$ having identical thermal-photon number \bar{n}_{PSGN} and $\eta_{\text{PSGN}} = \eta_0/5$. Noise from observable measurements may also be incorporated into the PSGN layers. The total PSGN is therefore thermal with error rate η_0 by assuming a small η_0 , which follows from the approximate additivity of thermal-noise channels of identical thermal photon number: $\mathcal{E}_{\text{therm}}^{(\eta_2, \bar{n})} \circ \mathcal{E}_{\text{therm}}^{(\eta_1, \bar{n})} \cong \mathcal{E}_{\text{therm}}^{(\eta_1 + \eta_2, \bar{n})}$ for small η_1 and η_2 (see Appendix A 2).

setting appropriate g and g' would be

$$\begin{aligned} g' &= \frac{1}{g\sqrt{1-\eta}}, \quad g \gg 2\sqrt{(2\ln 2)\frac{\bar{n}\eta}{1-\eta}} \quad (\text{thermal noise}), \\ g' &= \frac{1}{g}, \quad g \gg 2\sqrt{2\ln 2}\sigma \quad (\text{GDN}), \end{aligned} \quad (5)$$

where the two criteria for g reference the full-width-at-half-maxima of the respective Gaussian distributions.

In the special case where $\bar{n} = 0$, the thermal-noise channel is simply the loss channel. Then, $p(\beta, \beta^*) = \delta(\text{Re}\{\beta\})\delta(\text{Im}\{\beta\})$ and the mixture in (4) becomes ρ_{in} , which implies that any g and $g' = 1/(g\sqrt{1-\eta})$ exactly inverts the channel. Hence, the simplest setup that does this uses only one PSG [78]— $g = 1$ for instance. Otherwise, both thermal-noise and RDN channels can only be *asymptotically inverted* with $g \rightarrow \infty$ in such PSG-based setups.

Before we elaborate on how the amplifying PSG map may be realized nondeterministically in the next subsection, one can intuitively understand the asymptotic channel-inversion properties of PSGs through the help of Wigner-function diagrams supposing that such a map is (indirectly) realized. Figure 1 shows the possible fates of a nonclassical [99] input state undergoing different routes of operations, (b) one start-

ing with a linear amplification, that is $\mathcal{M}_{g>1}[\cdot] = g^{a^\dagger a} \cdot g^{a^\dagger a} / \text{tr}\{g^{a^\dagger a} \cdot g^{a^\dagger a}\}$, followed by thermal noise and ends with a linear attenuation $\mathcal{M}_{g'<1}$, and (c) another consisting of an amplifying PSG, then thermal noise and finally an attenuating PSG of the same $g > 1$ and $g' < 1$. Here, the important difference stems from the additional photon subtraction operations in PSGs. Without them, linear amplification alone simply increases the average photon number of the encoded state, leaving it even more susceptible to noise. The additional photon subtraction operations are crucial in strengthening the interference features of the state so that they become more noise-resilient—it is the *combined efforts* of photon subtraction, linear amplification and linear attenuation that achieves asymptotic channel inversion. (d) Reversing the PSG order results in no such noise-protective enhancement since an attenuating PSG on the input state dilutes the encoded quantum information. We emphasize that such interference fortification is only possible through nondeterministic implementation of the amplifying PSG. This provides a mechanism-based understanding that may be viewed as “trajectory cancellation” [78].

C. Error mitigation with PSGs and PEC

To circumvent the problem of a non-CP amplifying PSG that fundamentally prevents its direct experimental implementation, we can express ($g_\mu \equiv g/\mu$ and $0 < \mu < 1$)

$$\mathcal{M}_{\text{PSG}, g>1}[\rho_{\text{in}}] = \sum_{k=0}^{\infty} \underbrace{\mathcal{N}_{g_\mu} \frac{(-1 + g^{-2})^k}{(-1 + \mu^{-2})^k}}_{\equiv \omega_k} K_{\mu,k} \rho_{\text{in}}(g_\mu) K_{\mu,k}^\dagger \quad (6)$$

where $\mathcal{N}_{g_\mu} = \text{tr}\{g_\mu^{a^\dagger a} \rho_{\text{in}} g_\mu^{a^\dagger a}\}$, $\rho_{\text{in}}(g_\mu) = g_\mu^{a^\dagger a} \rho_{\text{in}} g_\mu^{a^\dagger a} / \mathcal{N}_{g_\mu}$ and the Kraus operators $K_{\mu,k} = \sqrt{(-1 + \mu^{-2})^k / k!} a^k \mu^{a^\dagger a}$ constitute $\mathcal{M}_{\text{PSG}, \mu < 1}$. That is, the unphysical amplifying PSG is exactly equivalent to a linear combination of Kraus operations from a deterministic attenuating PSG on a linearly-amplified state $\rho_{\text{in}}(g_\mu)$ (see Fig. 2), where the coefficient ω_k is known given some accurate estimate of \mathcal{N}_{g_μ} (see ** in Alg. 1). Such a linear amplification is *necessarily probabilistic* [100, 101] and may be carried out using quantum scissors that requires only linear optics and Fock resource states [63, 102], although alternative schemes exist for Gaussian states and certain classes of their superpositions [16, 103–108].

To proceed, we realize that a typical goal in quantum-information and computation tasks is to acquire expectation values of some observable $O = \sum_l |o_l\rangle \langle o_l|$, where $|o_l\rangle \langle o_l|$ are states that can be measured through a feasible circuit-sampling scheme. These, for instance, could be the eigenstates of O , in which case o_l correspond to its eigenvalues, or those that span the operator subspace containing O .

In this perspective, based on (6), we can apply an error-mitigation strategy known as *probabilistic error cancellation* (PEC) that would allow us to realize the map $\mathcal{M}_{\text{PSG}, g' < 1} \circ \mathcal{E} \circ \mathcal{M}_{\text{PSG}, g > 1}$ through measurement-outcome sampling and

probabilistically invert both the thermal-noise and RDN channels. More precisely, PEC mitigates estimation errors of $\langle O \rangle_{\text{out}} = \text{tr}\{\rho_{\text{out}} O\}$ for the noisy ρ_{out} in Eq. (4):

$$\begin{aligned} \langle O \rangle_{\text{out}} &= \sum_{k=0}^{\infty} \sum_{l=0}^{\infty} \omega_k o_l p_{kl}, \quad p_{kl} = \langle o_l | \sigma_k | o_l \rangle, \\ \sigma_k &= \sum_{k'=0}^{\infty} K_{g',k'} \mathcal{E}[K_{\mu,k} \rho_{\text{in}}(g_\mu) K_{\mu,k}^\dagger] K_{g',k'}^\dagger, \end{aligned} \quad (7)$$

where p_{kl} is the joint probability of measuring $K_{\mu,k}$ and o_l ($\sum_{k,l} p_{kl} = 1$). From (4), the larger the g , the more complete noise cancellation shall be.

Thus, the employment of PEC turns the unfeasible problem of coherently obtaining ρ_{out} in (4) into a feasible, albeit indirect, solution of mitigating errors in the measured expectation values through circuit sampling and classical postprocessing. For a finite sampling copy number N , the output expectation value $\langle O \rangle_{\text{out}}$ is estimated by some numerical estimator $\widehat{\langle O \rangle}_{\text{out}}$ that is random according to the collected measurement data, where the desired situation is that $\widehat{\langle O \rangle}_{\text{out}}$ is statistically close to the target expectation value $\langle O \rangle_{\text{targ}} = \text{tr}\{\rho_{\text{in}} O\}$, here evaluated with the noiseless target $\rho_{\text{targ}} = \rho_{\text{in}}$. The figure of merit for statistical quality that we shall adopt is the *mean squared-error* (MSE): $\mathcal{D} = \mathbb{E} \left[\left(\widehat{\langle O \rangle}_{\text{out}} - \langle O \rangle_{\text{targ}} \right)^2 \right]$, where $\mathbb{E}[\cdot]$ denotes the data average. In the large- N limit, we would like this estimator to be *consistent*, that is $\widehat{\langle O \rangle}_{\text{out}} \rightarrow \langle O \rangle_{\text{targ}}$.

We are left with deciding on the value of μ to execute the *PSG-PEC protocol*. In the infinite- N limit, it is obvious that any choice of μ gives the same $\langle O \rangle_{\text{out}}$ as $\mathcal{M}_{\text{PSG}, g > 1}[\rho]$ only depends on g and not how one portions this amplifying PSG map. For any finite N , however, the value of μ does affect the sampling error \mathcal{D} .

D. Optimal PSG-PEC estimators

We take p_{kl} to be joint probabilities of a multinomial distribution for some fixed N , which is a very common experimental scenario. One might then naïvely replace p_{kl} in the first equality of (7) by ν_{kl} , which is the relative frequency of measuring $K_{\mu,k}$ and o_l ($\sum_{k,l} \nu_{kl} = 1$) and regard the resulting sum to be the estimator. This is a fallacy because $\langle O \rangle_{\text{out}}$ is generally a *constrained* expectation value. For instance, when $O = \rho_{\text{targ}}$ is a pure target state, we have the fidelity $\mathcal{F} = \text{tr}\{\rho_{\text{targ}} \rho_{\text{out}}\}$, which is clearly constrained between 0 and 1. However, it is evident that $\sum_{k,l} \omega_k o_l \nu_{kl}$ is a random number that obeys no such physical constraints and, thus, cannot be a meaningful estimator.

Fortunately, for a constrained $a \leq \langle O \rangle_{\text{out}} \leq b$, the immediate fix is to define

$$\begin{aligned} \widehat{\langle O \rangle}_{\text{out}} &= \Theta(a - r) a + \Theta(r - b) b + \Theta(r - a) \Theta(b - r) r, \\ r &= \sum_{k,l} \omega_k o_l \nu_{kl} \equiv (\boldsymbol{\omega} \otimes \mathbf{o}) \cdot \boldsymbol{\nu}, \end{aligned} \quad (8)$$

as its corresponding constrained PSG-PEC estimator, where $\Theta(x)$ is the Heaviside step function that gives the desired constraining properties— $\langle \widehat{O} \rangle_{\text{out}} = a$ when $r < a$ and $\langle \widehat{O} \rangle_{\text{out}} = b$ if $r > b$. The relevant MSE reads

$$\mathcal{D} = \underbrace{\text{Var}[\langle \widehat{O} \rangle_{\text{out}}]}_{\text{variance}} + \underbrace{\left(\mathbb{E}[\langle \widehat{O} \rangle_{\text{out}}] - \langle O \rangle_{\text{targ}} \right)^2}_{\text{noise and statistical bias}}, \quad (9)$$

which, for values of N such that (B3) holds, is defined by

$$\begin{aligned} \mathbb{E}[\langle \widehat{O} \rangle_{\text{out}}] &= \frac{a+b}{2} + \frac{B-a}{2} \text{erf}\left(\frac{B-a}{\sqrt{2A}}\right) \\ &\quad - \frac{b-B}{2} \text{erf}\left(\frac{b-B}{\sqrt{2A}}\right) \\ &\quad + \sqrt{\frac{A}{2\pi}} \left[e^{-\frac{(B-a)^2}{2A}} - e^{-\frac{(b-B)^2}{2A}} \right], \\ \mathbb{E}[\langle \widehat{O} \rangle_{\text{out}}^2] &= \frac{a^2+b^2}{2} + \frac{A+B^2-a^2}{2} \text{erf}\left(\frac{B-a}{\sqrt{2A}}\right) \\ &\quad + \frac{A+B^2-b^2}{2} \text{erf}\left(\frac{b-B}{\sqrt{2A}}\right) \\ &\quad + \sqrt{\frac{A}{2\pi}} \left[e^{-\frac{(B-a)^2}{2A}} (B+a) - e^{-\frac{(b-B)^2}{2A}} (B+b) \right], \end{aligned} \quad (10)$$

where $A = \chi \cdot (\mathbf{Q} - \mathbf{q}\mathbf{q}) \cdot \chi / N$, $B = \chi \cdot \mathbf{q} \cdot \chi = \omega \otimes \mathbf{o}$ and

$$\mathbf{Q} = \begin{pmatrix} p_{11} & 0 & \cdots & 0 & 0 & \cdots & 0 \\ 0 & p_{12} & \cdots & 0 & 0 & \cdots & 0 \\ \vdots & \vdots & \ddots & \vdots & \vdots & \ddots & \vdots \\ 0 & 0 & \cdots & p_{21} & 0 & \cdots & 0 \\ 0 & 0 & \cdots & 0 & p_{22} & \cdots & 0 \\ \vdots & \vdots & \vdots & \vdots & \vdots & \ddots & \vdots \end{pmatrix}, \quad \mathbf{q} = \begin{pmatrix} p_{11} \\ p_{12} \\ \vdots \\ p_{21} \\ p_{22} \\ \vdots \end{pmatrix}. \quad (11)$$

As a sanity check, when the constraints are lifted ($a \rightarrow -\infty$ and $b \rightarrow \infty$), all error functions (erf) approach unity and we have $\mathbb{E}[\langle \widehat{O} \rangle_{\text{out}}] = B = \sum_{k,l} \omega_k o_l p_{kl} = \langle O \rangle_{\text{out}}$ and $\mathbb{E}[\langle \widehat{O} \rangle_{\text{out}}^2] = A + B^2 = A + \langle O \rangle_{\text{out}}^2$, which are precisely the first and second moments of the unconstrained estimator for multinomial data, so that $\mathcal{D} = A + (\langle O \rangle_{\text{out}} - \langle O \rangle_{\text{targ}})^2$. It is straightforward to see that this expression also holds when $N \gg 1$ based on the fact that $\text{erf}(x/\kappa) \rightarrow \Theta(x)$ as $\kappa \rightarrow 0$, which tells us that both the unconstrained and constrained estimation lead to the same estimator in the large- N limit. For sufficiently large g , the second bias tends to zero.

With \mathcal{D} in (9) (derived in Appendix B), we now supply an answer to the optimal μ for PSG-PEC: this is the value that *minimizes* \mathcal{D} . We first realize that although there is μ dependence in both ω_k and p_{kl} , and thus χ , $B = \chi \cdot \mathbf{q} = \langle O \rangle_{\text{out}}$ is independent of μ by definition, so A is the only function of μ . If $\mu = 0$ or 1, $A = \infty = \mathcal{D}$, which means that the

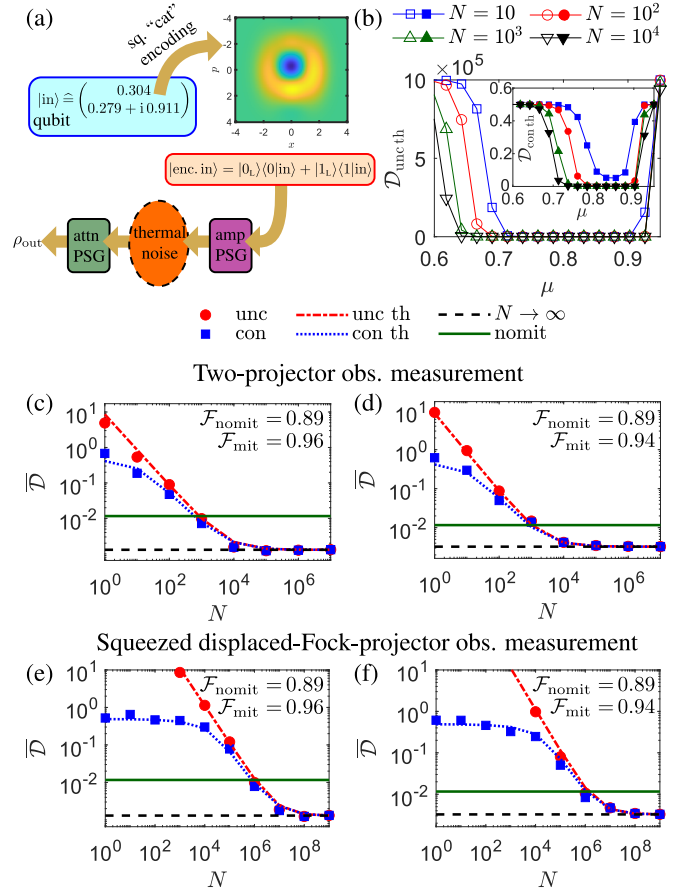


FIG. 3. (a) An example qubit state encoded in a 3dB-squeezed-“cat” code ($r = 0.345$, $\phi = 0$, $\alpha = 1$) is subjected to amplifying (amp, $g = 1.4$) and attenuating (attn, $g' = 0.855$) PSGs for mitigating thermal noise of $\eta = 0.05$ and $\bar{n} = 0.5$. (b) The landscapes of the theoretical MSE from (9) and (10) for both the unconstrained (unc) and constrained (con) estimators with respect to μ eventually flatten out as N increases (shown here for the two-projector measurement case). The corresponding μ_{opts} are used to formulate both unc and con estimators for $\langle \rho_{\text{targ}} \rangle_{\text{out}} = \text{tr}\{\rho_{\text{in}} \rho_{\text{out}}\}$ ($\rho_{\text{targ}} = \rho_{\text{in}}$). Averaged MSE curves for the (c,d) two-projector and (e,f) 64-squeezed-displaced-Fock-projector observable measurements are plotted. A total of 50 experiments are simulated to compute the average MSE $\overline{\mathcal{D}}$, (d,f) with and (c,e) without PSGN, where in (c,e), PSGN is distributed into five layers as in Fig. 2 such that $\eta_0 = 0.02$ and $\bar{n}_{\text{PSGN}} = 0.1$. All fitted curves are derived from the analytical expressions in (9) and (10). The fidelities in unmitigated ($\mathcal{F}_{\text{nomit}}$) and mitigated (\mathcal{F}_{mit}) scenarios, where the latter refers to the fidelity in the $N \rightarrow \infty$ limit, are reported. The black dashed and green solid lines respectively represent the bias $(\langle \rho_{\text{in}} \rangle_{\text{out}} - 1)^2$ with and without PSG mitigation. The larger number of projectors used in (e,f) consequently requires a larger N to approach the asymptotic \mathcal{F}_{mit} relative to (c,d).

global minimum for \mathcal{D} is within the interval $\mu \in (0, 1)$. As N increases, the landscape of \mathcal{D} over μ becomes flatter over a larger subinterval. Furthermore, the fact that N only appears in A as its reciprocal prefactor implies that the optimal μ that minimizes \mathcal{D} is *independent* of the sampling copy number N .

One can make use of (9) to obtain the global minimum μ_{opt} in the following way: if one expects the input state pre-

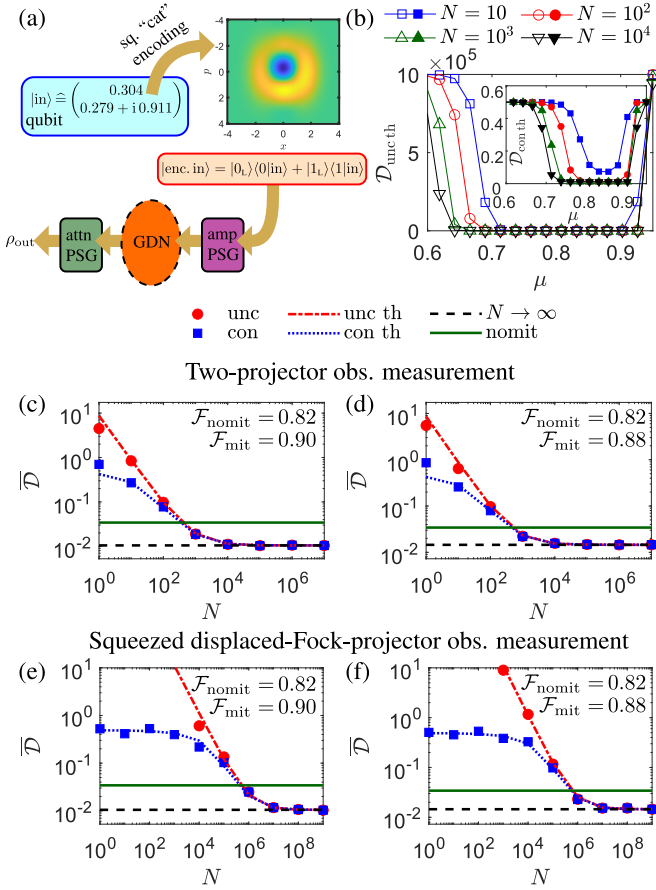


FIG. 4. PSG-PEC mitigation of GDN for a qubit state encoded in the same 3dB-squeezed-“cat” code presented in Fig. 3. To make contact with the parameters specifying the thermal-noise channel in Fig. 3, we set $\sigma = 0.281$ in accordance with the link between thermal noise and GDN through quantum-limited amplification described in Sec. II A. For this channel, $g = 1.4$ and $g' = 0.733$, while all other specifications follow those of Fig. 3.

pared is the ideal target state $\rho_{\text{targ}} = \rho_{\text{in}}$ (neglecting the existence of PSGN and other confounding errors) and knows the noise-channel parameters, then p_{kl} are the probabilities computed based on ρ_{targ} and noise channel. The corresponding μ_{opt} that minimizes \mathcal{D} in (9) with this target state can then be used to collect actual experimental data that are almost always contaminated with additional PSG noise and observable-measurement errors (collectively coined as PSGN) that would depend on the platform hardware. Here, these are modeled as thermal-noise layers sandwiching every key stages of the PSG-PEC mitigation scheme [see Fig. 2(c)]. This approximately accounts for realistic imperfections that are present in both the linear-amplification and attenuating-PSG stages, the implementation of both depends on actual hardware.

E. Complete procedure of PSG-PEC error mitigation

In summary, PSG-PEC follows the simple algorithm:

Algorithm 1 PSG-PEC

- 1: Determine the noise type and calibrate parameters η and \bar{n} .
 - 2: Set $g > 1$ that is reasonably large.
 - 3: Decide on the observable $O = \sum_l |o_l\rangle \langle o_l|$ of interest and feasible measurement outcomes $|o_l\rangle \langle o_l|$.
 - 4: Fix the number of copies N to be sufficiently large.
 - 5: Use (9) and (10) to obtain μ_{opt} , assuming ρ_{targ} and no PSGN.
 - 6: Set up the PSG-mitigation scheme with g, η, \bar{n} and μ_{opt} .
 - 7: Sample the multinomial distribution defined by N and p_{kl} s [see (7)], each being the probability of subtracting k photons and measuring state $|o_l\rangle \langle o_l|$, and collect data ν_{kl} of sample size N .
 - 8: Compute the error-mitigated $\langle \widehat{O} \rangle_{\text{out}}$ defined in (8), where ω_k is defined in (6). The constraints of $\langle \widehat{O} \rangle_{\text{out}}$ follow that of $\langle O \rangle_{\text{out}}$.
- ** An accurate estimate of $\mathcal{N}_{g\mu}$ is needed for the given input state. To this end, one may follow the steps above and sample any complete basis to find $\mathcal{N}_{g\mu}$ such that $\langle \widehat{1} \rangle_{\text{out}} \equiv 1$. This estimate would be accurate if N is sufficiently large.

Figures 3 and 4 present the respective performances of Alg. 1 in mitigating thermal noise and GDN on an example qubit encoded on squeezed-“cat” logical states $[S|0\rangle_L \propto S(|\alpha\rangle + |-\alpha\rangle), S|1\rangle_L \propto S(|\alpha\rangle - |-\alpha\rangle)]$, where $S = \hat{S}(z)$ is the squeeze operator of amplitude $z = re^{i\phi}$. The observable O is taken to be ρ_{targ} (fidelity estimation), with the ket $|\text{enc. in}\rangle$ characterizing ρ_{targ} stated in Figs. 3(a) and 4(a). Ideally, one may measure just the two projectors $|o_0\rangle \langle o_0| = |\text{enc. in}\rangle \langle \text{enc. in}|$ and $1 - |o_0\rangle \langle o_0|$. For a more practical means to estimate $\langle \rho_{\text{targ}} \rangle_{\text{out}}$ using squeezing, displacements and photon counting [109], we write

$$O = \rho_{\text{targ}} = \sum_{k=1}^K \sum_{n=0}^{\infty} SD(\beta_k) |n\rangle c_{kn} \langle n| D(\beta_k)^\dagger S^\dagger \quad (12)$$

as a linear combination of squeezed displaced-Fock projectors, the “ $|o_l\rangle \langle o_l|$ ”s (after normalization in p_{kl}), with varying weights c_{kn} , which are the “ o_l ”s. Appendix E 1 lists the required $\{\beta_k\}$ and $\{c_{kn}\}$ that constitute 64 squeezed displaced-Fock projectors ($K = 8$) for $z = 0.345 = 3\text{dB}$ and $\alpha = 1$. Note that in the limit $N \rightarrow \infty$, any observable measurement leads to the same asymptotic expectation-value estimator, as correctly confirmed by the figures.

As it turns out, the PSG-PEC mitigation scheme presented here in Sec. II is incapable of treating purely-dephasing channels. Instead, we propose a run-of-the-mill interferometer-based scheme that can coherently suppress such channels.

III. SUPPRESSING DEPHASING-NOISE CHANNELS

A. Dephasing channel

A purely-dephasing channel on a state ρ is modeled by

$$\mathcal{E}_{\text{deph}}^{(\gamma)}[\rho] = \int d\phi' p_\gamma(\phi') e^{i\phi' a^\dagger a} \rho e^{-i\phi' a^\dagger a} \quad (13)$$

describing a CPTP phase-randomization operation, where $p_\gamma(\phi')$ is the distribution of this mixture and $\gamma \geq 0$ quantifies

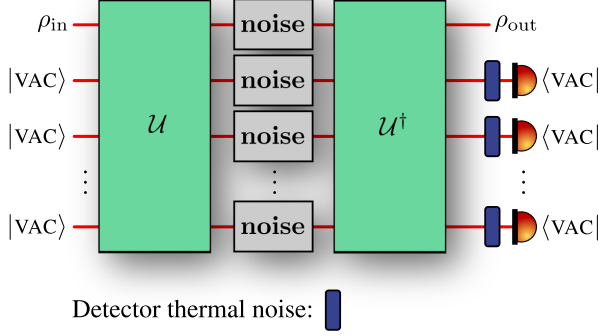


FIG. 5. The VMZ suppression scheme involving linear-optical elements and conditional vacuum measurements (implementable with on-off photodetectors in principle). The complete Mach-Zehnder interferometer is described by M -mode unitary transformations \mathcal{U} and \mathcal{U}^\dagger that both sandwich i.i.d. dephasing noise channels. More realistic considerations would involve additional thermal-noise channels before all photodetectors to account for measurement imperfections.

the dephasing strength. If $\gamma = 0$, $p_0(\phi') = \delta(\phi')$. A special class of dephasing channels, namely the central-Gaussian dephasing channels, are characterized by the central Gaussian distribution $p_\gamma(\phi') = e^{-\phi'^2/(2\gamma)}/\sqrt{2\pi\gamma}$.

Since in Appendix A (also in [49], for instance), we know that the thermal-noise map is a composition of the loss and quantum-limited amplification channels, the fact that $a^k e^{i\phi' a^\dagger a} = e^{i\phi' a^\dagger a} a^k e^{ik\phi'}$ implies that

$$\begin{aligned} \mathcal{E}_{\text{deph}}^{(\gamma)} \circ \mathcal{E}_{\text{therm}}^{(\eta, \bar{n})} &= \mathcal{E}_{\text{therm}}^{(\eta, \bar{n})} \circ \mathcal{E}_{\text{deph}}^{(\gamma)}, \\ \mathcal{E}_{\text{deph}}^{(\gamma)} \circ \mathcal{E}_{\text{GDN}}^{(\sigma)} &= \mathcal{E}_{\text{GDN}}^{(\sigma)} \circ \mathcal{E}_{\text{deph}}^{(\gamma)}; \end{aligned} \quad (14)$$

that is, thermal-noise channels and GDN channels independently commute with dephasing-noise channels for all channel parameters. For the same reason, the PSG map in Eq. (2) commutes with $e^{i\phi' a^\dagger a}$, such that PSG-PEC fails for *all* dephasing channels. Fortunately, there is a linear-optical strategy that suppresses such channels.

B. VMZ suppression scheme

We propose the *vacuum-based Mach-Zehnder* (VMZ) suppression scheme to coherently treat dephasing channels, as schematically laid out in Fig. 5. This comprises an initial M -mode beam splitter described by the unitary matrix \mathcal{U} that maps mode ladder operators a_j to their linear combinations: $a_j \mapsto a'_j = \sum_{k=1}^M \mathcal{U}_{jk} a_k$. This is not to be confused with the corresponding M -mode unitary evolution operator U_M acting on a single-mode state ρ and vacuum ancillas— $\rho_M = U_M[\rho \otimes (|\text{VAC}\rangle\langle\text{VAC}|)^{\otimes M-1}]U_M^\dagger$. This unitary map acts on the initially-prepared single-mode quantum state ρ_{in} , resulting in an M -mode output state ρ_M that next undergoes i.i.d. dephasing channels. At the end of the channels, another M -mode beam splitter described by \mathcal{U}^\dagger to com-

plete the mode interference. This Mach-Zehnder interferometric setup is then followed by vacuum measurements on $M - 1$ output ancillary modes. As these vacuum measurements are heralding, they collectively succeed with a non-unit probability. For any γ and M , this success probability is

$$p_{\text{VMZ}} = \text{tr} \left\{ U_M^\dagger \mathcal{E}_{\text{deph}}^{(\gamma)} [U_M [\rho_{\text{in}} \otimes (|\text{VAC}\rangle\langle\text{VAC}|)^{\otimes M-1}] U_M^\dagger] U_M \times \left[1 \otimes (|\text{VAC}\rangle\langle\text{VAC}|)^{\otimes M-1} \right] \right\}. \quad (15)$$

The M -mode unitary transformation \mathcal{U} (or equivalently operator U_M) can either be physically decomposed into a sequence of two-mode BSs and phase shifters (PSs) [110] or implemented in other more sophisticated architectures that are feasible in the laboratory [111–113]. The vacuum measurements may also be carried out with on-off detectors [64], or with superconducting-nanowire single-photon detectors (SNSPD) for higher efficiencies [114, 115]. Thus far, no specification regarding \mathcal{U} has been made for VMZ. We shall first show that there exists (at least) two classes of \mathcal{U} , namely the Hadamard transformations ($|\mathcal{U}_{jk}| = 1/\sqrt{M}$) and unitary two-design transformations (\mathcal{U} with Haar-random [116–119] first and second moments), that can facilitate the inversion of dephasing channels of *any* p_γ .

C. Inverting dephasing channels with infinitely many ancillas

To understand the channel-inversion capability of VMZ, it is instructive to analyze its action on an arbitrary coherent state $|\alpha\rangle\langle\alpha|$ and generalize the result to any state with the P function formalism. After the first beam splitter (\mathcal{U}), the coherent ket $|\alpha\rangle|\text{VAC}\rangle^{\otimes M-1} \mapsto |\mathcal{U}_{11}\alpha, \mathcal{U}_{21}\alpha, \dots, \mathcal{U}_{M1}\alpha\rangle$ is mapped into a product of coherent kets. The resultant state then undergoes i.i.d. dephasing, which from Eq. (13) is equivalent to an average over all possible phase-space rotations on each mode according to some distribution p_γ .

Let us suppose that the j th mode is subjected to a single phase-space rotation by an angle ϕ_j . Then

$$\begin{aligned} & e^{i\phi_1 a_1^\dagger a_1} e^{i\phi_2 a_2^\dagger a_2} \dots e^{i\phi_M a_M^\dagger a_M} |\mathcal{U}_{11}\alpha, \mathcal{U}_{21}\alpha, \dots, \mathcal{U}_{M1}\alpha\rangle \\ &= \left| \mathcal{U}_{11}\alpha e^{i\phi_1}, \mathcal{U}_{21}\alpha e^{i\phi_2}, \dots, \mathcal{U}_{M1}\alpha e^{i\phi_M} \right\rangle. \end{aligned} \quad (16)$$

The second beam splitter (\mathcal{U}^\dagger) then turns the output ket in (16) into $|s_1\alpha, s_2\alpha, \dots, s_M\alpha\rangle$, where the random complex number $s_l = \sum_{j=1}^M e^{i\phi_j} \mathcal{U}_{lj}^\dagger \mathcal{U}_{j1}$ and $\sum_{l=1}^M |s_l|^2 = 1$ owing to unitarity of \mathcal{U} or $\sum_{j=1}^M \mathcal{U}_{lj}^\dagger \mathcal{U}_{j\nu} = \delta_{l,\nu}$. The probabilistic conditional vacuum measurements lead to the final ket

$$|\alpha\rangle_\phi \propto |s_1\alpha\rangle e^{-\frac{1}{2}|\alpha|^2(1-|s_1|^2)} = s_1^{a^\dagger a} |\alpha\rangle\langle\alpha| s_1^{*a^\dagger a}. \quad (17)$$

Equation (17) highlights the underlying mechanism behind VMZ. The interferometric nature of VMZ sets up a mutual Mach-Zehnder interference on every independently-dephased optical modes between the beam splitters. Together with the $M - 1$ ancillary vacuum measurements, the entire

system essentially functions as a quantum adder that computes the sum (s_1) of squared magnitudes of random amplitudes that is encoded in a linear-attenuation operation as in Eq. (17) (since $|s_1| \leq 1$).

We are now ready to investigate the actual output state

$$\rho_{\text{out,VMZ}} = \frac{\overline{s_1^{a^\dagger a} \rho_{\text{in}} s_1^* a^\dagger a}}{\text{tr}\left\{s_1^{a^\dagger a} \rho_{\text{in}} s_1^* a^\dagger a\right\}}, \quad (18)$$

from the VMZ suppression scheme, where $\overline{f(\phi_1 \dots \phi_M)} = \int d\phi_1 p_\gamma(\phi_1) \dots \int d\phi_M p_\gamma(\phi_M) f(\phi_1 \dots \phi_M)$. For any finite M , Eq. (18) tells us that VMZ turns $\rho_{\text{out,VMZ}}$ into a heralded mixture of linearly-attenuated states. To proceed, we invoke Chebyshev's inequality, which states that (Appendix E2)

$$\text{pr}(|s_1 - \overline{s_1}| \geq \epsilon) \leq \frac{|\overline{s_1} - \overline{s_1}|^2}{\epsilon^2} = \frac{1 - |\lambda_\gamma|^2}{\epsilon^2} \sum_{j=1}^M |\mathcal{U}_{j1}|^4, \quad (19)$$

where $\lambda_\gamma = \overline{e^{i\phi_j}}$ is constant for all j and $|\lambda_\gamma| \leq 1$ just by the triangle inequality. Owing to the unitarity of \mathcal{U} , we note, also, that $\overline{s_1} = \lambda_\gamma \delta_{l,1}$. It turns out that there exist at least two classes of \mathcal{U} for which $Y \equiv \sum_{j=1}^M |\mathcal{U}_{j1}|^4 \rightarrow 0$ as $M \gg 1$. The first is the set of Hadamard transformations, where $|\mathcal{U}_{jk}|^2 = 1/M$ directly gives $Y = 1/M$. The second is the set of unitary two-design transformations, where it is shown in Appendix E3 that the two-design average $\overline{Y}^{\text{TD}} = 2/(M+1) \sim 1/M$, so that $Y \rightarrow 0$ typically as $M \rightarrow \infty$.

Therefore, in the asymptotic limit $M \rightarrow \infty$, for Hadamard and two-design interferometers, (19) implies that $s_l \rightarrow \lambda_\gamma \delta_{l,1}$ (the weak law of large numbers), which gives us the key result

$$\rho_{\text{out,VMZ}} \xrightarrow{M \rightarrow \infty} \frac{\lambda_\gamma^{a^\dagger a} \rho_{\text{in}} \lambda_\gamma^* a^\dagger a}{\text{tr}\left\{\lambda_\gamma^{a^\dagger a} \rho_{\text{in}} \lambda_\gamma^* a^\dagger a\right\}}, \quad (20)$$

where the success probability of VMZ is given by $p_{\text{VMZ}} = \text{tr}\left\{\lambda_\gamma^{a^\dagger a} \rho_{\text{in}} \lambda_\gamma^* a^\dagger a\right\} > 0$ and is typically not small even in the infinite- M regime. Finally, if $\lambda_\gamma = |\lambda_\gamma| e^{i\theta_\gamma}$, the rotated linear-amplification operation $\lambda_\gamma^{-a^\dagger a} = |\lambda_\gamma|^{-a^\dagger a} e^{-i\theta_\gamma a^\dagger a}$ may be further applied to probabilistically invert this channel.

In order to better appreciate (20), we focus on the central-Gaussian dephasing channel, for which $\lambda = e^{-\frac{\gamma}{2}}$. Such a channel also possesses a simple Kraus representation [Eq. (A11)], where each Kraus operator is accompanied with an exponential operator that is quadratic in $a^\dagger a$. Under this context, we remark that (20) may also be understood as an experimentally-feasible linearization of these quadratic exponents that permits successful inversion *without* requiring Kerr nonlinearities, where the latter is currently known to be technologically challenging [78]. It has been shown that linear optics suffices to approach the maximum success rate for linear amplification [102]. We shall next show that even with a finite M , VMZ already possesses dephasing-suppression qualities for weak dephasing strengths (small γ).

D. Suppression capabilities with finite number of ancillas

Let us analyze the circumstance with finite M by focusing on the popular *central-Gaussian* dephasing channel. For this channel, it is more expedient to express the *pure* input state $\rho_{\text{in}} = \sum_{m,n=0}^{\infty} |m\rangle \rho_{mn} \langle n|$ in the Fock basis to acquire the VMZ-suppressed output state

$$\rho_{\text{out,VMZ}} = \frac{\sum_{m,n=0}^{\infty} |m\rangle \rho_{mn} S_{mn} \langle n|}{\sum_{n=0}^{\infty} \rho_{nn} S_{nn}}, \quad (21)$$

where $S_{mn} = \overline{s_1^m s_1^{*n}}$ and $p_{\text{VMZ}} = \sum_{n=0}^{\infty} \rho_{nn} S_{nn}$. In the limit of small γ , with $w = 1 - \sum_{j=1}^M |\mathcal{U}_{j1}|^4$, the Kraus representation in (A11) and calculations in Appendix E4 give

$$S_{mn} \cong 1 - \frac{\gamma}{2} [(m+n)w + (m-n)^2(1-w)]. \quad (22)$$

To compare the quality of the suppressed output state relative to the unsuppressed one, we shall calculate the fidelities $\mathcal{F}_{\text{supp}} = \text{tr}\{\rho_{\text{in}} \rho_{\text{out,VMZ}}\}$ and $\mathcal{F}_{\text{nosupp}} = \text{tr}\{\rho_{\text{in}} \rho_{\text{out,no VMZ}}\}$, where $\rho_{\text{out,no VMZ}} = \sum_{m,n=0}^{\infty} |m\rangle \rho_{mn} e^{-\frac{\gamma}{2}(m-n)^2} \langle n|$. After invoking Taylor's expansion on the numerator and denominator of Eq. (21) via the use of (22), their difference reads

$$\Delta\mathcal{F} \equiv \mathcal{F}_{\text{supp}} - \mathcal{F}_{\text{nosupp}} = \frac{\gamma w}{2} \sum_{m,n=0}^{\infty} |\rho_{mn}|^2 (m-n)^2 \quad (23)$$

up to first order in γ , whence we find that $\mathcal{F}_{\text{supp}} \geq \mathcal{F}_{\text{nosupp}}$ for small γ . This states that for *any* beam splitter \mathcal{U} , dephasing suppression with VMZ is *always* successful in the weak-dephasing regime.

Equation (23) also provides us the opportunity to search for the optimal beam splitter \mathcal{U} that maximizes $\Delta\mathcal{F}$ in this regime. As w is the only function of \mathcal{U} , under the notation $p_j \equiv |\mathcal{U}_{j1}|^2$, this amounts to a simple minimization of w over \mathcal{U} under the unitarity constraint, which is equivalent to maximizing $1 - \sum_{j=1}^M p_j^2$ over p_j such that $\sum_{j=1}^M p_j^2 = 1$. Thus, the optimal solution is $p_j = 1/M$; that is, the optimal \mathcal{U} is Hadamard. Moreover, *any* Hadamard interferometer, not just a specific choice, can optimally suppress all central-Gaussian dephasing channels if γ is sufficiently small.

Interestingly, for *any* γ , one can also arrive at an approximate analytical formula for S_{mn} with $p_j = 1/M$ (denoted as $S_{\text{Had},mn}$). A very good approximation to $S_{\text{Had},mn}$ is in fact

$$S_{\text{Had},mn} \cong \tilde{S}_{mn} = \frac{e^{-\frac{\gamma}{2M}(m-n)^2}}{\left[1 + \frac{\gamma}{M}(m+n)\right]^{\frac{M-1}{2}}}. \quad (24)$$

Strictly speaking, the central limit theorem is applied to multinomial distributions [120] in order to derive (24), which normally requires $m, n \gg 1$. In this regime and the limit $M \rightarrow \infty$, (24) approaches $e^{-\frac{\gamma}{2}(m+n)}$ in accordance with Eq. (20), so that the discrepancy between $S_{\text{Had},mn}$ and \tilde{S}_{mn} tends to zero with increasing M . Details are found

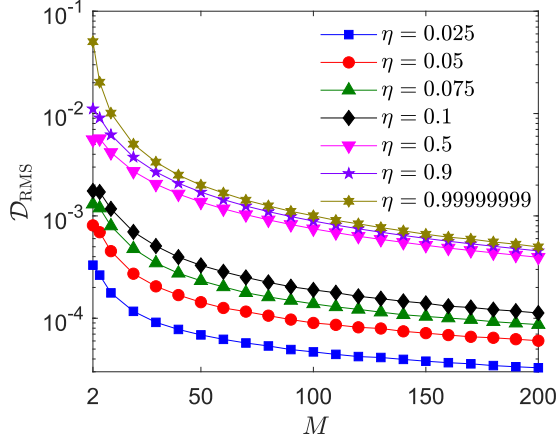


FIG. 6. The root-mean-square (RMS) distance $\mathcal{D}_{\text{RMS}} = \sqrt{\sum_{m,n=0}^9 (S_{\text{Had},mn} - \tilde{S}_{mn})^2 / 10^2}$ against M for different central-Gaussian dephasing channels of dephasing rate $\eta = 1 - e^{-\gamma}$. The largest \mathcal{D}_{RMS} occurs at $\gamma = \infty$ and $M = 2$, corresponding to $S_{\text{Had},mn} = \delta_{m,n} 4^{-m} \binom{2m}{m}$ [obtained from Eq. (E7) with $p_j = 1/M$] and $\tilde{S}_{mn} = \delta_{m,0} \delta_{n,0}$. Hence, $\max \mathcal{D}_{\text{RMS}} \cong 0.089$.

in Appendix E4 and E5. Rather surprisingly, Fig. 6 demonstrates remarkable accuracy of (24) even for small m and n .

IV. PERFORMANCE ON KNOWN BOSONIC CODES

We showcase the performance of error mitigation and suppression of noise channels for bosonic codes that are of general interest to quantum computation. For a given code, a single-qubit ket $|\text{qbit}\rangle = |0\rangle c_0 + |1\rangle c_1$ is encoded onto bosonic logical kets $|0\rangle_L$ and $|1\rangle_L$ to generate the input state $\rho_{\text{in}} = |\text{enc. in}\rangle \langle \text{enc. in}|$, with $|\text{enc. in}\rangle = |0\rangle_L c_0 + |1\rangle_L c_1$. All mitigation and suppression protocols serve to protect this input state against thermal noise, GDN, dephasing noise and their compositions. State fidelity is chosen as the figure of merit to quantify the mitigation and suppression qualities, since a high fidelity would naturally entail a good quality in either the coherent output state or any observable expectation-value estimation, be it at the logical or bosonic qubit level.

For a binary number b , in the Fock and position $\{|x\rangle_q\}$ bases, the four bosonic codes considered here that are often of interest in quantum information and computation are

- **Binomial** [3, 121], $\text{bin}(n, \kappa)$:

$$|b\rangle_L = 2^{-\frac{\kappa-1}{2}} \sum_{k=0}^{\lfloor \frac{\kappa-b}{2} \rfloor} |(2k+b)n\rangle \sqrt{\binom{\kappa}{2k+b}}.$$

- **n -component “cat”** [8, 46, 60, 61, 68], $\text{cat}(n, \alpha)$:

$$|b\rangle_L \propto \sum_{k=0}^{\infty} |n(k+b/2)\rangle \frac{\alpha^{n(k+b/2)}}{\sqrt{[n(k+b/2)]!}} \quad (\text{even } n).$$

- **Squeezed two-component “cat”** [76, 122–124], $\text{squat}(z, \alpha)$.
- **Finite-energy GKP** [2, 44, 125–128], $\text{gkp}(\Delta)$:

$$|b\rangle_L \propto \sum_{k=-\infty}^{\infty} e^{-\Delta^2 a^\dagger a} |(2k+b)\sqrt{\pi}\rangle_q.$$

Subsequently reported squeezing strength $|z| = r$ and Δ are in decibels (dB)— $r = r_{\text{dB}}(\ln 10)/20$ and $\Delta = 10^{-\Delta_{\text{dB}}/20}$. Numerical simulations are carried out with the help of Strawberry Fields [129, 130] and Mr Mustard [131] packages.

A. Mitigating thermal noise and GDN on bosonic codes

We measure the performance of PSG-PEC on all four bosonic codes by how they fare in estimating the fidelity between the target state $O = \rho_{\text{targ}}$ with respect to the mitigated output state in comparison to the unmitigated (noisy) output state. We shall compare asymptotic fidelities in the limit of large N . For thermal-noise and GDN channels, we will consider two scenarios in which noise is mitigated. The first scenario is one in which a quantum system, after being operated on by an amplifying PSG, undergoes idle noise as considered in Secs. II B and II C, either during storage and/or propagation stages of its journey in a quantum-information task. The target state $\rho_{\text{targ}} = \rho_{\text{in}}$ is the ideal input state.

In the second scenario [Fig. 7(b)], we would like to perform PSG-PEC on noise generated from an additional unitary gate U applied to the system *within* the passage that is in between the amplifying and attenuating PSGs (mitigation passage). This is an important application of PSG-PEC to quantum computation. The target state is then $\rho_{\text{targ}} = U \rho_{\text{in}} U^\dagger$. However, we caution that care must be taken to ensure that the gate U' inside the mitigation passage is properly adjusted so that it corresponds to the intended gate operation U . The two are generally not the same as $\mathcal{M}_{\text{PSG},g}[U \cdot U^\dagger] = U' \mathcal{M}_{\text{PSG},g}[\cdot] U'^\dagger \neq U \mathcal{M}_{\text{PSG},g}[\cdot] U^\dagger$ and a wrong choice of U' would result in low mitigated quality due to additional gate distortion by the PSG [Fig. 7(c)]. Single-mode gate noise is then modeled as two identical (thermal-noise or GDN) layers of noise rate $\eta/2$ before and after U' , where η is also the noise rate of the idle noise channel. Noise of a two-mode gate is modeled as two layers before U' and two after (all identical), each possessing a noise rate of $\eta/2$. For the given encoded ρ_{in} , fair performance comparisons between idle- and gate-noise scenarios can thus be made under the same total noise rate per mode when η is small (see Appendix A2).

We will focus on the universal gate-set $\mathcal{S} = \{D(\alpha), i^{a^\dagger a}, e^{i\chi q^3}, e^{i\chi' q} \otimes p\}$ [30, 132, 133] consisting of the displacement, Fourier, cubic and CX gates in this order. The modded gate U' for PSG-PEC mitigation is straightforward regarding the first two gates; that is, the pair $U = D(\alpha)$, $U' = D(g\alpha)$ for the displacement gate and $U = i^{a^\dagger a} = U'$ for the Fourier gate, both valid for a PSG of gain/loss factor g ,

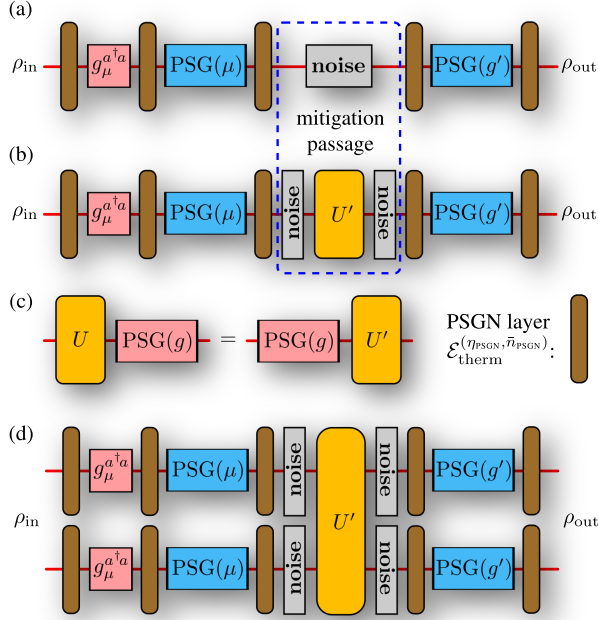


FIG. 7. Noise mitigation with PSG-PEC in two scenarios: a PSG-treated state that is either (a) idling or (b) subjected to a gate operation. (c) If the intended unitary-gate operation on ρ_{in} is U , then a proper gate modification (U') should be carried out to minimize, if not eradicate, gate distortion coming from the commutation through $g_{\mu}^{a^{\dagger}a}$ and $\text{PSG}(\mu)$, which would otherwise introduce unwanted excess errors in addition to gate noise. All diagrams refer to single-mode gate operations, which are easily generalized to multimode cases by employing independent PSG-mitigation setups for each mode. (d) Shown here is an example for a two-mode system.

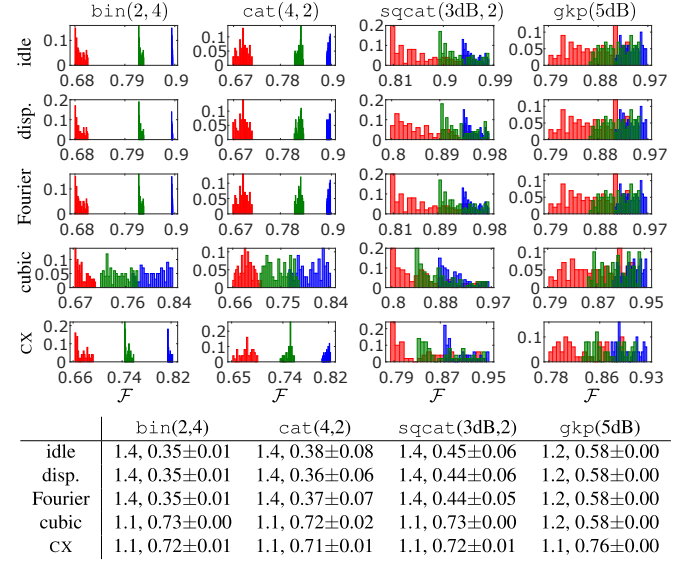
are respectively a result of Eq. (3) and the commutativity between a rotation gate and the PSG operation. The cubic phase gate and CX gate, on the other hand, do not exhibit easy forms of U' to our knowledge. The search for such a U' for these gates that either exactly nullifies or partially cancel PSG gate distortion is an interesting future work. Nevertheless, when χ and χ' are not too large, (multimode) PSG-PEC is still successful even with realistic imperfect operations as gate distortion by the amplifying PSG is not major.

In both idling and gate-operated scenarios, for either thermal noise or GDN, the general procedure for PSG-PEC is given in Alg. 1. Furthermore, the linear-amplification operation $g_{\mu_{\text{opt}}}^{a^{\dagger}a}$, being nondeterministic, succeeds with a certain probability that determines the success rate of our PSG-PEC mitigation protocol. We adopt the linear-optical recipe proposed in Ref. [102] that saturates the *maximum achievable* success probability, which was found to be

$$\max p_{\text{PSG-PEC}} = g_{\mu_{\text{opt}}}^{-2} = (g/\mu_{\text{opt}})^{-2} \quad (25)$$

in that reference ($g > 1$) and is also the one that we take to benchmark the protocol for all bosonic codes. Finally, noisy gates are modeled as the gate U' sandwiched between two identical noise channels (be it thermal or GD) of rate $\eta/2$.

(a) Thermal noise (idle and gates): $\eta = 0.05$, $\bar{n} = 0.5$



(b) GDN (idle and gates): $\sigma = 0.281$ for $\eta = 0.05$ and $\bar{n} = 0.5$

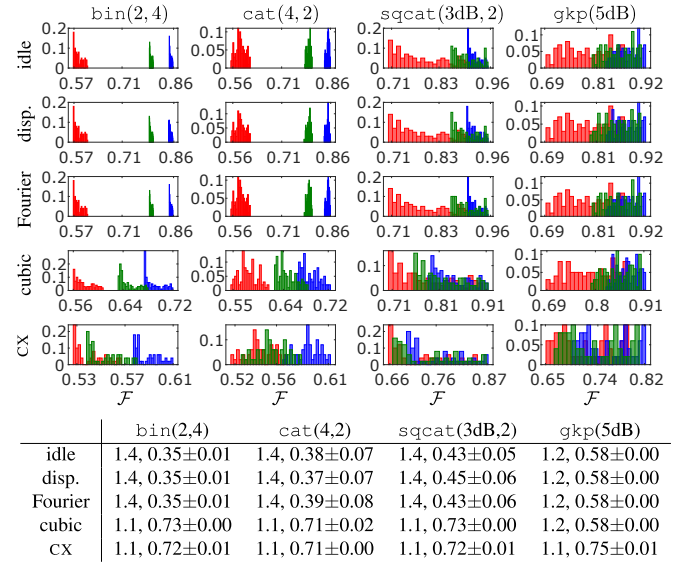


FIG. 8. The large- N estimated fidelities with PSG-PEC mitigation in the absence (blue) and presence (green) of PSGN ($\eta_{\text{PSGN}} = 0.02$, $\bar{n}_{\text{PSGN}} = 0.1$), and without (red) are shown here for both (a) thermal noise and (b) GDN. All histograms are normalized in probability. A total of 100 random single-mode ρ_{in} s for each bosonic code are generated by encoding qubit states chosen uniformly from the Bloch sphere to simulate the PSG-PEC performance with the idle, $D(0.27 + 0.55i)$, $i^{a^{\dagger}a}$ and $e^{i0.05 q^3}$ operations. For the CX gate $e^{i0.1 q_1 p_2}$, 50 random two-mode ρ_{in} s per code are generated from product states, where one input mode (CX target) is the vacuum state and the other (CX control) a random encoded-qubit state. Both g and *state-averaged* $\max p_{\text{PSG-PEC}}$ from Eq. (25), along with its standard deviation, are given, where smaller g values are applied to both cubic and CX gates to avoid significant gate distortion. All red and blue histograms for both idle and Fourier-gate operations are *almost* identical since all channels are additive for small η (such as those considered here) and $i^{a^{\dagger}a}$ commutes with the PSG and both the thermal-noise and GDN channels based on the commutation relation $a^k i^{a^{\dagger}a} = i^{a^{\dagger}a} (ia)^k$.

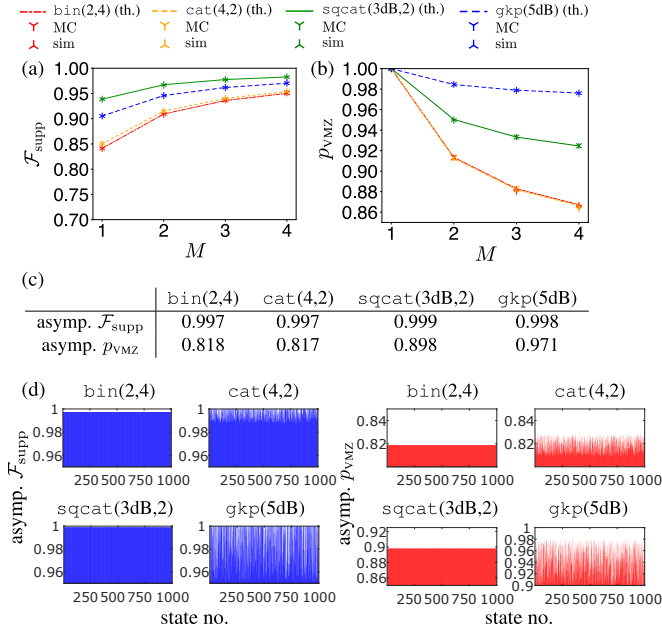


FIG. 9. VMZ suppression of an idling central-Gaussian dephasing channel ($\eta = 1 - e^{-\gamma} = 0.05$) for bosonic codes encoding a randomly-chosen qubit ket $|\text{qbit}\rangle = |0\rangle 0.765 + |1\rangle (0.641 + 0.058i)$, using a Hadamard \mathcal{U} of M modes ($M - 1$ ancillary modes). The (a) suppression fidelity $\mathcal{F}_{\text{supp}}$ and (b) success probability p_{VMZ} are plotted, where $M = 1$ signifies the absence of dephasing suppression (no VMZ). The analytical approximation (th.) in (24) and success-probability formula are compared with both numerical computation of the summations in Eq. (E7) that explicitly defines S_{mn} through Monte Carlo multinomial sampling (MC) and simulations using Strawberry Fields and Mr Mustard (sim). (c) Up to the first decimal place, these finite- M values are very close to the asymptotic ones ($M \rightarrow \infty$) already at $M = 2$. (d) Moreover, for 1000 randomly-chosen qubits (uniform on the Bloch sphere) encoded in these bosonic codes, both asymp. $\mathcal{F}_{\text{supp}}$ and asymp. p_{VMZ} are extremely high, if not near-unity. Here, all vacuum measurements suffer no additional thermal noise for simplicity.

In this way, the *total gate-noise channel* (composition of the two sandwiching channels) is the same as the idle noise channel of rate η for small η due to channel additivity (see Appendix A 2), which ensures an equal-footing comparison of PSG-PEC performance during idling and gate operations.

Figure 8(a) presents the performance of PSG-PEC ($g > 1$) in mitigating thermal noise for idle and universal gate operations on all four bosonic codes. For all tested encoded-qubit states, *all* unmitigated estimated fidelities are lower than mitigated ones, with or without PSGN. In particular, a smaller g is applied to gkp in order to simulate this code with the same Fock-space dimension as other codes for the same computation efficiency ($d = 20$ per mode for CX and $d = 60$ for single-mode gates). The fact that with such low values of g , PSG-PEC still permits significant improvements in fidelity-estimation accuracy is testament to the practical utility of PSG-PEC in mitigating thermal-noise and GDN channels. The relatively high best-case $p_{\text{PSG-PEC}}$, achievable with linear-optical methods [102], motivates the search for evermore effi-

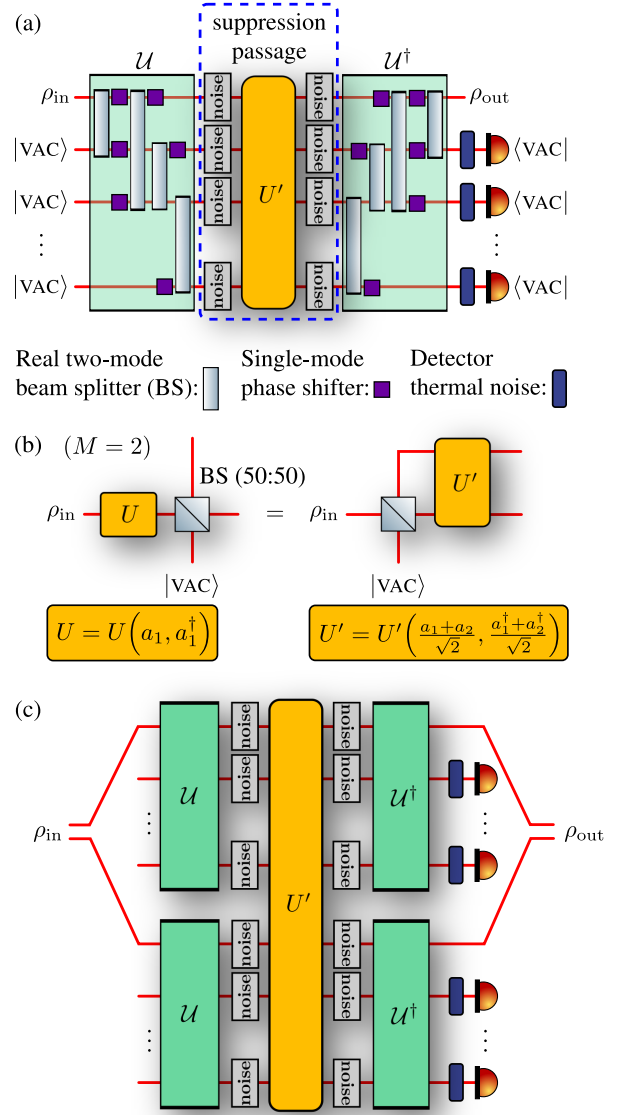


FIG. 10. Single-mode gate modification in VMZ suppression to avoid interferometric gate distortion. (a) From [111], every \mathcal{U} can be implemented with real, two-mode BSs and PSs (phase-space rotators). (b) For $M = 2$, a typical Hadamard \mathcal{U} corresponds to the balanced two-mode BS. The U' of the (noiseless) gate operation U on the input state ρ_{in} is, thus, a function of linear combinations of ladder operators on different modes. For larger M , U' is further altered by PSs. (c) Multimode gate-noise suppression (shown here for two input modes) is carried out using independent VMZ setups.

cient ways to perform linear-amplification operations.

Mitigating GDN with $\sigma = \sqrt{\eta(1 + \bar{n})/(1 - \eta)}$ using $\eta = 0.05$ and $\bar{n} = 0.5$ set in Fig. 8(a), as shown in Fig. 8(b), proves to be more difficult with the same values of g . The overall estimated fidelities (mitigated or not) are lower than when noise channels are thermal for the same η and \bar{n} . The performance on the cubic phase gate and CX gate tell us that PSG-PEC is especially prone to even slight PSG imperfections in the case of GDN.

TABLE I. Gate modifications for VMZ of $M = 2$, where $\text{BS}_{1,2}(\vartheta, \varphi) = \exp(\vartheta(e^{i\varphi}a_1a_2^\dagger - e^{-i\varphi}a_1^\dagger a_2))$ describes a real BS, here taken to be balanced, $\widetilde{\text{BS}}_{1,2} \equiv \text{BS}_{1,2}(\pi/4, 0)$ for simplicity, $R_j(\varphi) = \exp(i\varphi a_j^\dagger a_j)$ the rotation operator and all subscripts refer to the mode numbers acted upon. For single-mode gates, the second and third columns respectively list the modified gates according to $\widetilde{\text{BS}}_{1,2}U = V'\widetilde{\text{BS}}_{1,2}$ and $R_1(\varphi)U = V'R_1(\varphi)$. For two-mode gates, they coincide with $\widetilde{\text{BS}}_{1,2}\widetilde{\text{BS}}_{3,4}U = V''\widetilde{\text{BS}}_{1,2}\widetilde{\text{BS}}_{3,4}$ and $R_1(\varphi)R_2(\varphi')U = V''R_1(\varphi)R_2(\varphi')$. Regarding the CX gate, modes 1 and 3 refer to the inputs, and 2 and 4 the BS ancillas.

U	$U' = V'$	$U' = V''$
$D_1(\alpha)$	$D_1(\alpha/\sqrt{2})D_2(\alpha\sqrt{2})$	$D_1(\alpha e^{i\varphi})$
$i^{\dagger}a_1$	$i^{\frac{1}{2}}(a_1^\dagger + a_2^\dagger)(a_1 + a_2)$	$i^{\dagger}a_1$
$e^{i\chi q_1^n}$	$e^{i\frac{\chi}{2^{n/2}}(q_1 + q_2)^n}$	$e^{i\chi(q_1 \cos \varphi + p_1 \sin \varphi)^n}$
$e^{i\chi' q_1 p_3}$	$e^{i\frac{\chi'}{2}(q_1 + q_2)(p_3 + p_4)}$	$\exp(i\chi'(q_1 \cos \varphi + p_1 \sin \varphi) \times (p_3 \cos \varphi' - q_3 \sin \varphi'))$

B. Suppressing dephasing noise on bosonic codes

We first look at scenario one in which the encoded qubit is subjected to an idling central-Gaussian dephasing channel. Figure 9 plots the convergence of both the VMZ-suppression fidelity $\mathcal{F}_{\text{supp}}$ and success probability p_{VMZ} corresponding to a randomly-chosen qubit that is encoded on all four bosonic codes. This encoded qubit is one of the many other tested random ones that yields an $\mathcal{F}_{\text{supp}}$ and p_{VMZ} which are already close to the asymptotic values ($M \rightarrow \infty$) even when M is small, up the first decimal place. Moreover, over the qubit Bloch sphere, the distributions of $\mathcal{F}_{\text{supp}}$ and p_{VMZ} are both generally extremely high for these tested bosonic codes. From numerical observations, typically, the increase in $\mathcal{F}_{\text{supp}}$ is largest in going from $M = 1$ (no VMZ suppression) to $M = 2$.

When a single-mode gate U are applied to the encoded qubit (scenario two), then the attempt to suppress purely-dephasing channels coming from the gate operation by the VMZ scheme would also result in gate distortion. From Ref. [111], the beam splitter \mathcal{U} may be decomposed into real two-mode BSs and single-mode phase shifters [Fig. 10(a,b)]. The gate distortion is therefore coming from commuting U through these linear-optical passive components. Fortunately, there exist convenient algebraic forms of U' needed inside the suppression passage. Such prescriptions may be generalized to multimode gate operations [Fig. 10(c)]. Table I lists the corresponding U' s for all U s in the universal gate-set \mathcal{S} when $M = 2$. Noisy U' s are, likewise, modeled in exactly the same way as in Sec. IV A. Here, the dephasing-noise layers sandwiching the noisy U' , be it a single- or two-mode gate, also each possesses a rate $\eta/2$ per mode such that the total gate-dephasing channel is that of the idle-dephasing channel of rate η for small η as per Appendix A 2.

Figure 11 lists the performance of the VMZ suppression scheme on all bosonic codes. Remarkably, just using a simple

Central-Gaussian dephasing noise (idle and gates): $\eta = 1 - e^{-\gamma} = 0.05$

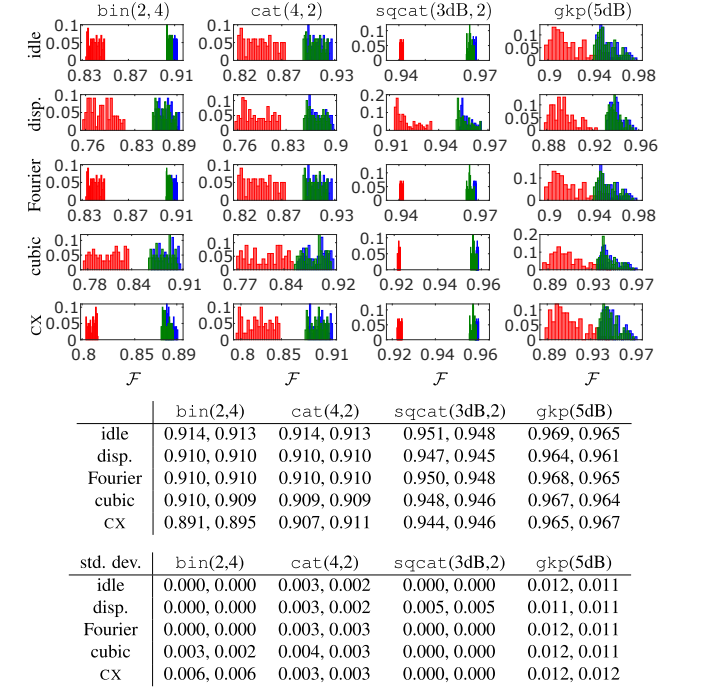


FIG. 11. Output fidelities with Hadamard-VMZ dephasing suppression ($M = 2$) in the absence (blue) and presence (green) of detector thermal noise ($\eta_{\text{DET}} = 0.05$, $\bar{n}_{\text{DET}} = 0.1$), and without (red). The operations considered are idle, $D(0.27 + 0.55i)$, $i^{\dagger}a$, $e^{i0.05q^3}$ and $e^{i0.5q_1p_2}$, where ρ_{inS} are generated in the same way as in Fig. 8. VMZ success probabilities in the absence (p_{VMZ} , left) and presence (\tilde{p}_{VMZ} , right) of detector thermal noise are listed. Just like PSG-PEC, all red and blue histograms for both idle and Fourier-gate operations are *almost* identical since the dephasing channel is additive for small η and $i^{\dagger}a$ clearly commutes with this noise channel.

balanced BS ($M = 2$ or single ancillary mode) with no additional phases, significant improvements in output-state fidelities is still achievable. For reasonably-small detector imperfections, the suppressed fidelities remain almost unchanged.

C. Suppressive mitigation of noise-channel compositions

We take this moment to reiterate some crucial notes on the PSG and VMZ schemes. Recall that the PSG is unable to offer any error mitigation on dephasing channels. At the same time, we show in Appendix C that the VMZ protocol cannot suppress *both* thermal noise and GDN. More generally, however, noise channels may be modeled as a composition of different kinds. An example is the composition of a thermal-noise channel and a dephasing channel, which is also known to be degradable [37]. The commutativity between thermal-noise and dephasing-noise channels, and between GDN and dephasing-noise channels, as in (14), tells us that any other complicated compositions of thermal-noise (or GDN) and dephasing channels may be simplified to such a two-layered composition. Our error-mitigation and suppres-

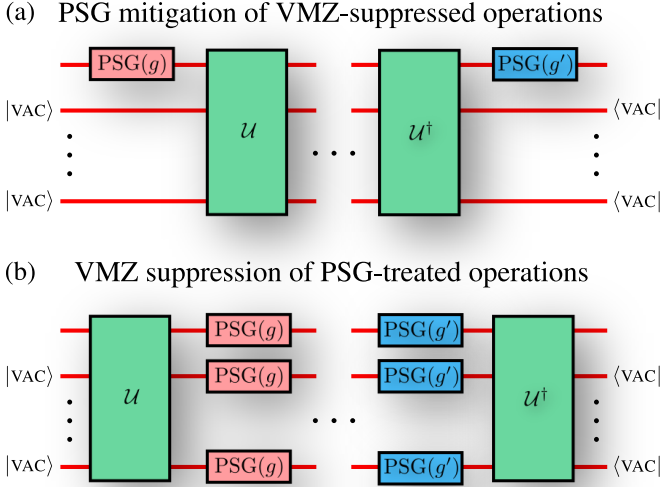


FIG. 12. Compatibility between PSG-mitigation and VMZ-suppression schemes: (a) and (b) are equivalent for *any* U , g and g' .

sion strategies would prove useful if they can be utilized to suppressively mitigate these noise-channel compositions.

Indeed, it is possible to simultaneously implement PSG-PEC and VMZ-suppression protocols to treat such noise compositions. According to Fig. 12, one may either (a) sandwich the multimode VMZ interferometer with PSGs or, instead, (b) sandwich multimodal PSGs with the VMZ interferometer. It turns out (see Appendix D) that both configurations are identical, which tells us that PSG-mitigation and VMZ-suppression schemes are *mutually compatible*, so that we can conveniently carry out both schemes without paying attention to their ordering. Advice on the forms of U' depending on the gate operation U that are given in Secs. IV A and IV B may be heeded to cope with gate distortions.

In short, the *hybrid PSG-VMZ scheme* is equivalent to PSG-PEC mitigation carried out on the VMZ-suppressed passage as shown in Fig. 12(a), where the final mitigation procedure is once again described in Alg. 1. As a key demonstration of the hybrid PSG-VMZ protocol for suppressive mitigation of composite noise channels, Fig. 13 presents the PEC error-mitigation results on both the idle and cubic-phase-gate operations for thermal-dephasing and GD-dephasing noise. Here, all dephasing noise are assumed to be central-Gaussian. The best-case success probability for this hybrid scheme is:

$$\max p_{\text{PSG-VMZ}} = (g/\mu_{\text{opt}})^{-2} \sum_{k=0}^{\infty} p_k p_{\text{VMZ},k}, \quad (26)$$

where p_k is the probability of subtracting k photons and $p_{\text{VMZ},k}$ is the VMZ success rate when this happens. We see that when PSGN and thermally-noisy vacuum detectors are considered in the hybrid protocol, the difficulty in mitigating GD-dephasing noise manifests itself as possible lower mitigated fidelities in comparison to the unmitigated ones, which

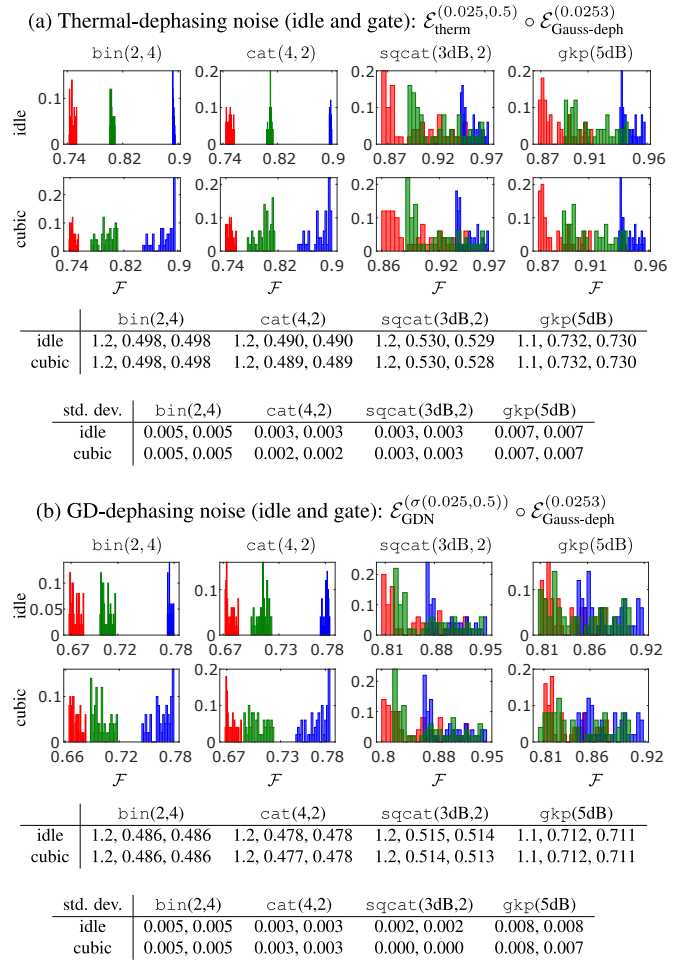


FIG. 13. Suppressive mitigation of (a) thermal-dephasing noise and (b) GD-dephasing noise for the idle operation and the cubic phase gate $e^{i0.02q^3}$. Here the two channel-noise layers are equally distributed in η so that the *total noise rate* remains as 0.05, with $\gamma = 0.0253$ corresponding to the dephasing rate of 0.025. The triplet of values g , $\max p_{\text{PSG-VMZ}}$ and $\max \tilde{p}_{\text{PSG-VMZ}}$ (accounting for the vacuum-measurement thermal noise in the VMZ part), together with the standard deviations of both types of success probabilities over 50 states are quoted. In contrast to the unmitigated fidelities (red), all PEC mitigated ones, be it in the ideal case (blue) or in the presence of PSGN *and* vacuum-detection thermal noise (green), are always higher for thermal-dephasing noise. On the other hand, the same sort of difficulty in mitigating GD-dephasing noise as exhibited in Fig. 8(b) exists.

originates from the GDN part of the composite noise channel.

V. DISCUSSION

In the age of NISQ devices, where information-processing and computation tasks are carried out in relatively noisy environments, it is of paramount importance to be able to protect quantum information from the influence of noise using feasible resources and methodologies. In this work, we have successfully made use of linear-optical techniques to mitigate

and suppress common noise that plague qubits encoded onto quantum bosonic codes.

In particular, using gadgets involving photon subtraction, linear attenuation and amplification, all realizable with passive linear components, photodetectors and manageable non-classical resource states, we showed that thermal noise and general random displacement noise can be asymptotically mitigated from measured expectation values. We further developed proper constrained statistics theory to improve the error-mitigation quality. Even more interestingly, we proved that just by employing a straightforward multimode Mach-Zehnder interferometer and vacuum-state measurements, any purely-dephasing noise can be turned into a linear-attenuation channel, with an, often, high success probability when the number of modes is very large. This can then be, in principle, completely inverted with a linear amplification operation. Such an inversion, previously thought to be accomplishable only with nonlinear optical elements, is now known to be doable linear optically. Moreover, for any finite number of modes and dephasing rate that is not too large, we show that such an interferometric scheme always suppresses the commonly-considered central-Gaussian dephasing channel and that a uniform multimode beam splitter is optimal for this purpose. In the simplest case of a single ancillary mode, a balanced beam-splitter-based interferometer suffices and can lead to significant state-fidelity improvement for reasonable noise parameters. Last, but not the least, we found that both the mitigation and suppression schemes are mutually compatible with each other, so that they may be implemented simultaneously in any order to mitigate more realistic noise channels that are compositions of the aforementioned noise types, namely the thermal-dephasing and Gaussian-displacement-dephasing channels.

For common bosonic encodings, we numerically verified our established theoretical formalism and confirmed, indeed, that our linear-optical mitigation and suppression schemes can reduce errors due to idling noise channels. More importantly, we tested the schemes on universal gate-set operations and found that they are also effective in mitigating and suppressing gate noise. Furthermore, all results demonstrated that these protocols are robust to slight detector imperfections.

Owing to the recent advancement in experimental implementation of linear amplification at higher success rates and multimode interferometers, realization of the mitigation and suppression protocols presented here are becoming increasingly more feasible in practice. The possibility of implementing similar gadgets and measurements on superconducting systems, for instance, permits the possibility of their realization on platforms beyond quantum optics in the realm of bosonic quantum computing. In view of such versatility, this work finds immediate practical applications of noise mitigation and suppression on current quantum technologies.

VI. ACKNOWLEDGMENTS

We thank A. Taylor, H. Kwon, K. Park, N. Lo Piparo and O. Solodovnikova for fruitful discussions. This

work is supported by the National Research Foundation of Korea (NRF) grants funded by the Korean government (MSIT) (Grant Nos. 2023R1A2C1006115, NRF-2022M3K4A1097117, RS-2023-00237959 and RS-2024-00413957) via the Institute of Applied Physics at Seoul National University, the Institute of Information & Communications Technology Planning & Evaluation (IITP) grant funded by the Korea government (MSIT) (IITP-2021-0-01059 and IITP-20232020-0-01606), and the Brain Korea 21 FOUR Project grant funded by the Korean Ministry of Education.

Appendix A: Properties of the thermal-noise, GDN and dephasing channels

1. Definitions

The subsequent discussion relies on the complex Gaussian integration identity [134, 135]

$$\begin{aligned} & \int \frac{(d\beta)}{\pi} e^{-a|\beta|^2 + b_1\beta + b_2\beta^* + c_1\beta^2 + c_2\beta^{*2}} \\ &= \frac{1}{\sqrt{a^2 - 4c_1c_2}} \exp\left(\frac{ab_1b_2 + c_1b_2^2 + c_2b_1^2}{a^2 - 4c_1c_2}\right) \end{aligned} \quad (\text{A1})$$

for $\text{Re}\{a\} \geq |c_1 + c_2^*|$, providing an interesting alternative route through the use of the coherent-state basis in contrast to the usual covariance-matrix comparison of two Gaussian channels [136].

Both the loss and quantum-limited amplification channels may be defined in terms of Kraus operators inasmuch as

$$\begin{aligned} \mathcal{L}_\mu[\rho] &= \sum_{k=0}^{\infty} \frac{\mu^k}{k!} (1-\mu)^{a^\dagger a/2} a^k \rho a^\dagger k (1-\mu)^{a^\dagger a/2}, \\ \mathcal{A}_G[\rho] &= \frac{1}{G} \sum_{k=0}^{\infty} \frac{(1-G^{-1})^k}{k!} a^\dagger k G^{-a^\dagger a/2} \rho G^{-a^\dagger a/2} a^k. \end{aligned} \quad (\text{A2})$$

If $\mu = 1 - (1-\eta)/G$ and $G = 1 + \eta \bar{n}$, then it can be shown that $\mathcal{A}_G \circ \mathcal{L}_{1-(1-\eta)/G} = \mathcal{E}_{\text{therm}}^{(\eta, \bar{n})}$, where $\mathcal{L}_\eta = \mathcal{E}_{\text{therm}}^{(\eta, 0)}$. To see this, we observe what happens to an arbitrary coherent state under these CPTP maps. While it is simple to arrive at $\mathcal{L}_\mu[|\alpha\rangle\langle\alpha|] = |\sqrt{1-\mu}\alpha\rangle\langle\sqrt{1-\mu}\alpha|$, we look at the Husimi Q function of the final state:

$$\begin{aligned} Q(\beta, \beta^*) &= \langle\beta| \mathcal{A}_G \left[|\alpha\sqrt{1-\mu}\rangle\langle\alpha\sqrt{1-\mu}| \right] |\beta\rangle \\ &= \frac{1}{G} \sum_{k=0}^{\infty} \frac{(1-G^{-1})^k}{k!} |\beta|^{2k} e^{(G^{-1}-1)(1-\mu)|\alpha|^2} \\ &\quad \times e^{-|\beta - \alpha\sqrt{(1-\mu)G^{-1}}|^2} \\ &= \frac{1}{G} e^{-\frac{1}{G}|\beta - \alpha\sqrt{1-\eta}|^2}. \end{aligned} \quad (\text{A3})$$

From the connection

$$Q(\beta, \beta^*) = \int \frac{(d\beta')}{\pi} P(\beta', \beta'^*) e^{-|\beta' - \beta|^2} \quad (\text{A4})$$

between the Q and P functions [137], and the fact that $Q(\beta, \beta^*)$ is a Gaussian function, it is clear that $P(\beta, \beta^*)$ is also Gaussian if it were not highly singular. After recognizing that

$$\mathcal{E}_{\text{therm}}^{(\eta, \bar{n})} [|\alpha\rangle \langle \alpha|] = \int \frac{(d\beta)}{\pi} |\beta\rangle \frac{e^{-\frac{1}{\eta \bar{n}} |\beta - \alpha \sqrt{1-\eta}|^2}}{\eta \bar{n}} \langle \beta| \quad (\text{A5})$$

from (1), upon inserting the P function

$$P(\beta, \beta^*) = \frac{e^{-\frac{1}{\eta \bar{n}} |\beta - \alpha \sqrt{1-\eta}|^2}}{\eta \bar{n}} \quad (\text{A6})$$

of $\mathcal{E}_{\text{therm}}^{(\eta, \bar{n})} [|\alpha\rangle \langle \alpha|]$, we see that

$$\begin{aligned} Q(\beta, \beta^*) &= \frac{e^{-\frac{1-\eta}{\eta \bar{n}} |\alpha|^2 - |\beta|^2}}{\eta \bar{n}} \\ &\times \int \frac{(d\beta')}{\pi} e^{-\frac{1+\eta \bar{n}}{\eta \bar{n}} |\beta'|^2} e^{\left(\frac{\sqrt{1-\eta}}{\eta \bar{n}} \alpha^* + \beta^*\right) \beta'} + \text{c.c.} \\ &= \frac{e^{-\frac{1-\eta}{\eta \bar{n}} |\alpha|^2 - |\beta|^2}}{1 + \eta \bar{n}} e^{\frac{1}{\eta \bar{n} (1+\eta \bar{n})} |\alpha \sqrt{1-\eta} + \beta \eta \bar{n}|^2} \\ &= \frac{1}{G} e^{-\frac{1}{G} |\beta - \alpha \sqrt{1-\eta}|^2}. \end{aligned} \quad (\text{A7})$$

By the same token, using Eq. (A1), we may verify that $\mathcal{A}_{1/(1-\eta)} [\mathcal{E}_{\text{therm}}^{(\eta, \bar{n})} [|\alpha\rangle \langle \alpha|]] = \mathcal{E}_{\text{GDN}}^{(\sigma)} [|\alpha\rangle \langle \alpha|]$ through comparison of state Q functions. After some steps of calculations, the Q function of the left-hand side is

$$\langle \beta | \mathcal{A}_{1/(1-\eta)} [\mathcal{E}_{\text{therm}}^{(\eta, \bar{n})} [|\alpha\rangle \langle \alpha|]] | \beta \rangle = \frac{1-\eta}{1+\eta \bar{n}} e^{-\frac{1-\eta}{1+\eta \bar{n}} |\alpha - \alpha'|^2}, \quad (\text{A8})$$

whereas that of the right-hand side is

$$\langle \beta | \mathcal{E}_{\text{GDN}}^{(\sigma)} [|\alpha\rangle \langle \alpha|] | \beta \rangle = \frac{1}{1+\sigma^2} e^{-\frac{1}{1+\sigma^2} |\alpha - \alpha'|^2}, \quad (\text{A9})$$

so that $\sigma^2 = \eta(1+\bar{n})/(1-\eta)$.

Lastly, the central-Gaussian dephasing channel leads to

$$\int d\phi \frac{e^{-\frac{\phi^2}{2\gamma}}}{\sqrt{2\pi\gamma}} e^{i\phi a^\dagger a} |m\rangle \langle n| e^{-i\phi a^\dagger a} = |m\rangle \langle n| e^{-\frac{\gamma}{2}(m-n)^2} \quad (\text{A10})$$

on the operator element $|m\rangle \langle n|$. It is easy to see that the Taylor expansion $e^{-\frac{\gamma}{2}(m-n)^2} = e^{-\frac{\gamma}{2}m^2} \sum_{k=0}^{\infty} \frac{\gamma^k}{k!} (mn)^k e^{-\frac{\gamma}{2}n^2}$ straightforwardly supplies the Kraus representation

$$\mathcal{E}_{\text{Gauss-deph}}^{(\gamma)} [\rho] = \sum_{k=0}^{\infty} \frac{\gamma^k}{k!} e^{-\frac{\gamma}{2}(a^\dagger a)^2} (a^\dagger a)^k \rho (a^\dagger a)^k e^{-\frac{\gamma}{2}(a^\dagger a)^2}. \quad (\text{A11})$$

2. Approximate channel additivity in noise parameters

We study the result of composing two channels, beginning with thermal channels, where an application of (A1) yields

$$\begin{aligned} &\mathcal{E}_{\text{therm}}^{(\eta_2, \bar{n})} \circ \mathcal{E}_{\text{therm}}^{(\eta_1, \bar{n})} [|\alpha\rangle \langle \alpha|] \\ &= \int \frac{(d\beta)}{\pi} |\beta\rangle \frac{e^{-\frac{1-\eta_1}{\eta_1 \bar{n}} |\alpha|^2 - \frac{1}{\eta_2 \bar{n}} |\beta|^2}}{(\eta_1 + \eta_2 - \eta_1 \eta_2) \bar{n}} \langle \beta| \\ &\quad \times e^{\frac{\eta_1 \eta_2}{(\eta_1 + \eta_2 - \eta_1 \eta_2) \bar{n}} \left| \frac{\sqrt{1-\eta_1}}{\eta_1} \alpha + \frac{\sqrt{1-\eta_2}}{\eta_2} \beta \right|^2}. \end{aligned} \quad (\text{A12})$$

Now, for small η_1 and η_2 , since

$$\begin{aligned} \eta_1 + \eta_2 - \eta_1 \eta_2 &\cong \eta_1 + \eta_2, \\ \frac{1-\eta_1}{\eta_1} \left(\frac{\eta_2}{\eta_1 + \eta_2 - \eta_1 \eta_2} - 1 \right) &\cong -\frac{1-\eta_1-\eta_2}{\eta_1 + \eta_2}, \\ \frac{1}{\eta_2} \left[(1-\eta_2) \frac{\eta_1}{\eta_1 + \eta_2 - \eta_1 \eta_2} - 1 \right] &\cong -\frac{1}{\eta_1 + \eta_2}, \end{aligned} \quad (\text{A13})$$

it is clear that for any $\bar{n} \geq 0$

$$\mathcal{E}_{\text{therm}}^{(\eta_2, \bar{n})} \circ \mathcal{E}_{\text{therm}}^{(\eta_1, \bar{n})} \cong \mathcal{E}_{\text{therm}}^{(\eta_1 + \eta_2, \bar{n})} \text{ for small } \eta_1, \eta_2. \quad (\text{A14})$$

Next, for the GDN channels, the sleight-of-hand substitution $u = \beta + \beta'$ and $u' = \beta - \beta'$ corresponding to a Jacobian of determinant equal to *four* followed by the employment of (A1) on the u' integration yields,

$$\begin{aligned} &\mathcal{E}_{\text{GDN}}^{(\sigma_2)} \circ \mathcal{E}_{\text{GDN}}^{(\sigma_1)} [|\alpha\rangle \langle \alpha|] \\ &= \int \frac{(d\beta)}{\pi \sigma_2^2} \int \frac{(d\beta')}{\pi \sigma_1^2} |\alpha + \beta + \beta'\rangle e^{-\frac{|\beta'|^2}{\sigma_1^2} - \frac{|\beta|^2}{\sigma_2^2}} \langle \alpha + \beta + \beta'| \\ &= \int \frac{(du)}{\pi(\sigma_1^2 + \sigma_2^2)} |\alpha + u\rangle e^{-\frac{|u|^2}{\sigma_1^2 + \sigma_2^2}} \langle \alpha + u|, \end{aligned} \quad (\text{A15})$$

which clearly means that

$$\mathcal{E}_{\text{GDN}}^{(\sigma_2)} \circ \mathcal{E}_{\text{GDN}}^{(\sigma_1)} = \mathcal{E}_{\text{GDN}}^{(\sqrt{\sigma_1^2 + \sigma_2^2})} \text{ for any } \sigma_1 \text{ and } \sigma_2, \quad (\text{A16})$$

the standard consequence of convolving two Gaussian distributions. If $\sigma_j^2 = \eta_j(1+\bar{n})/(1-\eta_j)$, then for small η_1 and η_2 ,

$$\begin{aligned} \sigma_1^2 + \sigma_2^2 &= (1+\bar{n}) \frac{\eta_1 + \eta_2 - 2\eta_1 \eta_2}{1 - \eta_1 - \eta_2 - \eta_1 \eta_2} \\ &\cong (1+\bar{n}) \frac{\eta_1 + \eta_2}{1 - \eta_1 - \eta_2}. \end{aligned} \quad (\text{A17})$$

In other words,

$$\mathcal{E}_{\text{GDN}}^{(\sigma(\eta_2, \bar{n}))} \circ \mathcal{E}_{\text{GDN}}^{(\sigma(\eta_1, \bar{n}))} \cong \mathcal{E}_{\text{GDN}}^{(\sigma(\eta_1 + \eta_2, \bar{n}))} \text{ for small } \eta_1, \eta_2. \quad (\text{A18})$$

Finally, the statement

$$\mathcal{E}_{\text{Gauss-deph}}^{(\gamma_2)} \circ \mathcal{E}_{\text{Gauss-deph}}^{(\gamma_1)} = \mathcal{E}_{\text{Gauss-deph}}^{(\gamma_1 + \gamma_2)} \text{ for any } \gamma_1 \text{ and } \gamma_2 \quad (\text{A19})$$

follows immediately from the actions

$$\begin{aligned} & \mathcal{E}_{\text{Gauss-deph}}^{(\gamma_2)} \circ \mathcal{E}_{\text{Gauss-deph}}^{(\gamma_1)} [|m\rangle \langle n|] \\ &= \mathcal{E}_{\text{Gauss-deph}}^{(\gamma_2)} \left[|m\rangle e^{-\frac{\gamma_1}{2}(m-n)^2} \langle n| \right] \\ &= |m\rangle e^{-\frac{\gamma_1 + \gamma_2}{2}(m-n)^2} \langle n| \end{aligned} \quad (\text{A20})$$

on the arbitrary Fock element $|m\rangle \langle n|$. In terms of the dephasing rate $\eta = 1 - e^{-\gamma}$, the Reader is invited to verify that

$$\mathcal{E}_{\text{Gauss-deph}}^{(\eta_2)} \circ \mathcal{E}_{\text{Gauss-deph}}^{(\eta_1)} = \mathcal{E}_{\text{Gauss-deph}}^{(\eta_1 + \eta_2)} \text{ for small } \eta_1, \eta_2. \quad (\text{A21})$$

To conclude, all these noise channels are additive in the regime of small noise rates η .

Appendix B: Constrained parameter estimation

Let $x = \sum_{j=1}^M w_j \nu_j = \mathbf{w} \cdot \boldsymbol{\nu}$, where w_j s are just weights of the sum over all multinomial relative frequencies ν_j . If one defines a new random variable $y = \Theta(x-a)\Theta(b-x)x + \Theta(a-x)a + \Theta(x-b)b$ that is limited to the range $[a, b]$, where Θ is the Heaviside step function, then the task of interest here is the calculation of $\mathbb{E}[y^n]$, where

$$y^n = \Theta(x-a)\Theta(b-x)x^n + \Theta(a-x)a^n + \Theta(x-b)b^n. \quad (\text{B1})$$

Because $\Theta(0) = 1/2$ by convention, we may consider a and $b > a$ to respectively be ever so slightly (up to numerical precision) smaller and larger than the lower and upper limits of the actual range of $\sum_{j=1}^M w_j p_j = \mathbf{w} \cdot \mathbf{p}$. Using the famous integral representation

$$\Theta(x) = \lim_{\epsilon \rightarrow 0^+} \int \frac{d\tau}{2\pi i} \frac{e^{ix\tau}}{\tau - i\epsilon}, \quad (\text{B2})$$

and taking a sufficiently large copy number N and invoking the central limit theorem [Eq. (4.20) of [138]],

$$\mathbb{E}\left[e^{i\lambda \mathbf{w} \cdot \boldsymbol{\nu}}\right] \cong e^{-\frac{A}{2}\lambda^2 + iB\lambda}, \quad (\text{B3})$$

where $A = \mathbf{w} \cdot (\mathbf{P} - \mathbf{p}\mathbf{p}) \cdot \mathbf{w}/N$, $B = \mathbf{w} \cdot \mathbf{p}$ (remembering that $a < B < b$) and both $\mathbf{P} = \text{diag}(\mathbf{p})$ and $\mathbf{p}\mathbf{p}$ are matrices characterizing the multinomial distribution. From hereon, we will incessantly exploit the deceptively simple result

$$\frac{1}{i(a - i\epsilon)} = \int_0^\infty du e^{-iu(a - i\epsilon)} \quad (\epsilon > 0). \quad (\text{B4})$$

We first settle the second and third terms in (B1):

$$\begin{aligned} \mathbb{E}[\Theta(a-x)a^n] &= a^n \lim_{\epsilon \rightarrow 0^+} \int \frac{d\tau}{2\pi} \frac{e^{ia\tau}}{\tau - i\epsilon} \mathbb{E}\left[e^{-i\tau \mathbf{w} \cdot \boldsymbol{\nu}}\right] \\ &= a^n \int_0^\infty du \int \frac{d\tau}{2\pi} e^{-\frac{A}{2}\tau^2 + i(a-B-u)\tau} \\ &= a^n \int_0^\infty \frac{du}{\sqrt{2\pi A}} e^{-\frac{1}{2A}(u-a+B)^2} \\ &= \frac{a^n}{2} \text{erfc}\left(\frac{B-a}{\sqrt{2A}}\right), \end{aligned} \quad (\text{B5})$$

$$\mathbb{E}[\Theta(x-b)b^n] = \frac{b^n}{2} \text{erfc}\left(\frac{b-B}{\sqrt{2A}}\right). \quad (\text{B6})$$

It, then, follows that

$$\begin{aligned} \mathbb{E}[y^n] &= \frac{a^n + b^n}{2} - \frac{a^n}{2} \text{erf}\left(\frac{B-a}{\sqrt{2A}}\right) - \frac{b^n}{2} \text{erf}\left(\frac{b-B}{\sqrt{2A}}\right) \\ &+ \lim_{\epsilon, \epsilon' \rightarrow 0^+} \int \frac{d\tau}{2\pi i} \frac{e^{-ia\tau}}{\tau - i\epsilon} \int \frac{d\tau'}{2\pi i} \frac{e^{ib\tau'}}{\tau' - i\epsilon'} \\ &\times \left(-i \frac{d}{d\lambda}\right)^n \mathbb{E}\left[e^{i\lambda \mathbf{w} \cdot \boldsymbol{\nu}}\right] \Big|_{\lambda=\tau-\tau'}. \end{aligned} \quad (\text{B7})$$

Specifically when $n = 1$ and 2, for instance,

$$\begin{aligned} -i \frac{d}{d\lambda} \mathbb{E}\left[e^{i\lambda \mathbf{w} \cdot \boldsymbol{\nu}}\right] &\cong (B + iA\lambda) e^{-\frac{A}{2}\lambda^2 + iB\lambda}, \\ \left(-i \frac{d}{d\lambda}\right)^2 \mathbb{E}\left[e^{i\lambda \mathbf{w} \cdot \boldsymbol{\nu}}\right] &\cong (A + B^2 + 2iAB\lambda - A^2\lambda^2) \\ &\times e^{-\frac{A}{2}\lambda^2 + iB\lambda}. \end{aligned} \quad (\text{B8})$$

Since the exponential terms are analytic functions of τ and τ' , the answers to $\mathbb{E}[y]$ and $\mathbb{E}[y^2]$ may be subsequently obtained by handling the double integrals inasmuch as

$$\begin{aligned} \mathbb{E}[y] &= \frac{a+b}{2} - \frac{a}{2} \text{erf}\left(\frac{B-a}{\sqrt{2A}}\right) - \frac{b}{2} \text{erf}\left(\frac{b-B}{\sqrt{2A}}\right) \\ &+ B \lim_{\epsilon, \epsilon' \rightarrow 0^+} \int \frac{d\tau}{2\pi i} \frac{e^{-ia\tau}}{\tau - i\epsilon} \int \frac{d\tau'}{2\pi i} \frac{e^{ib\tau'}}{\tau' - i\epsilon'} \\ &\times e^{-\frac{A}{2}(\tau - \tau')^2 + iB(\tau - \tau')} \\ &+ iA \lim_{\epsilon, \epsilon' \rightarrow 0^+} \int \frac{d\tau}{2\pi i} \frac{e^{-ia\tau}}{\tau - i\epsilon} \int \frac{d\tau'}{2\pi i} \frac{e^{ib\tau'}}{\tau' - i\epsilon'} \\ &\times (\tau - \tau') e^{-\frac{A}{2}(\tau - \tau')^2 + iB(\tau - \tau')}. \end{aligned} \quad (\text{B9})$$

The first double integral simplifies to

$$\begin{aligned} & \int_0^\infty du \int_0^\infty du' \int \frac{d\tau}{2\pi} e^{i(B-a-u)\tau} \\ & \times \int \frac{d\tau'}{2\pi} e^{-\frac{A}{2}(\tau - \tau')^2 + i(b-B-u')\tau'} \\ &= \int_0^\infty \frac{du}{\sqrt{2\pi A}} \int_0^\infty du' \delta(b-a-u-u') e^{-\frac{1}{2A}(u'+B-b)^2}, \end{aligned} \quad (\text{B10})$$

where we point out that the delta function yields a nonzero answer only when $u \leq b - a$, which gives rise to

$$\begin{aligned} & \int_0^{b-a} \frac{du}{\sqrt{2\pi A}} e^{-\frac{1}{2A}(u+a-B)^2} \\ &= \frac{1}{2} \left[\operatorname{erf}\left(\frac{B-a}{\sqrt{2A}}\right) + \operatorname{erf}\left(\frac{b-B}{\sqrt{2A}}\right) \right]. \end{aligned} \quad (\text{B11})$$

Similarly, the second double integral turns out to be

$$\begin{aligned} & \int_0^\infty du' \int \frac{d\tau}{2\pi i} e^{i(B-a)\tau} \\ & \quad \times \int \frac{d\tau'}{2\pi} e^{-\frac{A}{2}(\tau-\tau')^2 + i(b-B-u')\tau'} \\ & - \int_0^\infty du \int \frac{d\tau}{2\pi} e^{i(B-a-u)\tau} \\ & \quad \times \int \frac{d\tau'}{2\pi i} e^{-\frac{A}{2}(\tau-\tau')^2 + i(b-B)\tau'} \\ &= \int_0^\infty du' \int \frac{d\tau}{2\pi i} e^{-i(u'+a-b)\tau} \frac{1}{\sqrt{2\pi A}} e^{-\frac{1}{2A}(u'+B-b)^2} \\ & \quad - \int_0^\infty du \int \frac{d\tau}{2\pi i} e^{-i(u+a-b)\tau} \frac{1}{\sqrt{2\pi A}} e^{-\frac{1}{2A}(b-B)^2} \\ &= \frac{1}{i\sqrt{2\pi A}} \left[e^{-\frac{1}{2A}(B-a)^2} - e^{-\frac{1}{2A}(b-B)^2} \right]. \end{aligned} \quad (\text{B12})$$

So,

$$\begin{aligned} \mathbb{E}[y] &= \frac{a+b}{2} + \frac{B-a}{2} \operatorname{erf}\left(\frac{B-a}{\sqrt{2A}}\right) - \frac{b-B}{2} \operatorname{erf}\left(\frac{b-B}{\sqrt{2A}}\right) \\ & \quad + \sqrt{\frac{A}{2\pi}} \left[e^{-\frac{1}{2A}(B-a)^2} - e^{-\frac{1}{2A}(b-B)^2} \right]. \end{aligned} \quad (\text{B13})$$

If $a \rightarrow -\infty$ and $b \rightarrow \infty$, then $\mathbb{E}[y] \rightarrow B$. Also, since $\operatorname{erf}(x/k) \rightarrow 2\Theta(x) - 1$ when $k \rightarrow 0$, as $N \rightarrow \infty$, $A \rightarrow 0$ and $\mathbb{E}[y] \rightarrow a\Theta(a-B) + b\Theta(B-b) + B\Theta(b-B)\Theta(B-a) = B$ as it should be.

To obtain $\mathbb{E}[y^2]$, we need to evaluate

$$\begin{aligned} & \lim_{\epsilon, \epsilon' \rightarrow 0^+} \int \frac{d\tau}{2\pi i} \frac{e^{-ia\tau}}{\tau - i\epsilon} \int \frac{d\tau'}{2\pi i} \frac{e^{ib\tau'}}{\tau' - i\epsilon'} \\ & \quad \times (\tau - \tau')^2 e^{-\frac{A}{2}(\tau - \tau')^2 + iB(\tau - \tau')} \\ &= \lim_{\epsilon' \rightarrow 0^+} \int \frac{d\tau'}{2\pi i} \frac{e^{i(b-B)\tau'}}{\tau' - i\epsilon'} \int \frac{d\tau}{2\pi i} e^{-\frac{A}{2}(\tau - \tau')^2 + i(B-a)\tau} \\ & \quad + \lim_{\epsilon \rightarrow 0^+} \int \frac{d\tau}{2\pi i} \frac{e^{i(B-a)\tau}}{\tau - i\epsilon} \int \frac{d\tau'\tau'}{2\pi i} e^{-\frac{A}{2}(\tau - \tau')^2 + i(b-B)\tau'} \\ & \quad - 2 \int \frac{d\tau}{2\pi i} e^{-ia\tau} \int \frac{d\tau'}{2\pi i} e^{ib\tau'} e^{-\frac{A}{2}(\tau - \tau')^2 + iB(\tau - \tau')}, \end{aligned} \quad (\text{B14})$$

where the first integral gives

$$\begin{aligned} & \frac{e^{-\frac{1}{2A}(B-a)^2}}{A^{3/2}\sqrt{2\pi}} \lim_{\epsilon' \rightarrow 0^+} \int \frac{d\tau'}{2\pi i} \frac{e^{i(b-a)\tau'}}{\tau' - i\epsilon'} (B-a - iA\tau') \\ &= \frac{e^{-\frac{1}{2A}(B-a)^2}}{A^{3/2}\sqrt{2\pi}} [\Theta(b-a)(B-a) - A\delta(b-a)] \\ &= \frac{e^{-\frac{1}{2A}(B-a)^2}}{A^{3/2}\sqrt{2\pi}} (B-a), \end{aligned} \quad (\text{B15})$$

the second integral is simply the first upon replacing $B-a$ with $b-B$, and, finally, the third being

$$\begin{aligned} & -2 \int \frac{d\tau}{2\pi i} e^{-ia\tau} \int \frac{d\tau'}{2\pi i} e^{ib\tau'} e^{-\frac{A}{2}(\tau' - \tau)^2 - iB(\tau' - \tau)} \\ &= \sqrt{\frac{2}{\pi A}} e^{-\frac{1}{2A}(b-B)^2} \delta(b-a) = 0. \end{aligned} \quad (\text{B16})$$

After all is said and done,

$$\begin{aligned} \mathbb{E}[y^2] &= \frac{a^2 + b^2}{2} + \frac{A + B^2 - a^2}{2} \operatorname{erf}\left(\frac{B-a}{\sqrt{2A}}\right) \\ & \quad + \frac{A + B^2 - b^2}{2} \operatorname{erf}\left(\frac{b-B}{\sqrt{2A}}\right) \\ & \quad + \sqrt{\frac{A}{2\pi}} \left[e^{-\frac{(B-a)^2}{2A}} (B+a) - e^{-\frac{(b-B)^2}{2A}} (B+b) \right]. \end{aligned} \quad (\text{B17})$$

Again, when $a \rightarrow -\infty$ and $b \rightarrow \infty$, $\mathbb{E}[y^2] \rightarrow A + B^2$. For very large N , we have that $\mathbb{E}[y^2] \rightarrow a^2\Theta(a-B) + b^2\Theta(B-b) + (A+B^2)\Theta(b-B)\Theta(B-a) = A + B^2$.

Appendix C: Thermal-noise- and GDN-suppression incapability with VMZ

We shall analyze the action of VMZ on coherent states and generalize it to arbitrary states under the P function formalism. Let us first apply the M -mode unitary transformation described by the unitary matrix \mathcal{U} on the coherent state $|\alpha\rangle \langle\alpha|$:

$$\begin{aligned} |\alpha\rangle \langle\alpha| &\mapsto e^{\alpha \sum_{j=1}^M \mathcal{U}_{1j} a_j^\dagger} |\text{VAC}\rangle e^{-|\alpha|^2} \langle\text{VAC}| e^{\alpha^* \sum_{j=1}^M \mathcal{U}_{1j}^* a_j} \\ &= |\alpha \mathcal{U}_{11}, \dots, \alpha \mathcal{U}_{1M}\rangle \langle\alpha \mathcal{U}_{11}, \dots, \alpha \mathcal{U}_{1M}|, \end{aligned} \quad (\text{C1})$$

where $\sum_{j=1}^M \mathcal{U}_{1j} \mathcal{U}_{jk}^\dagger = \delta_{1,k}$. After the thermal-noise map,

$$\begin{aligned} & |\alpha \mathcal{U}_{11}, \dots, \alpha \mathcal{U}_{1M}\rangle \langle\alpha \mathcal{U}_{11}, \dots, \alpha \mathcal{U}_{1M}| \\ &\mapsto \int \frac{(d\boldsymbol{\beta})}{\bar{n}^M \pi^M} e^{\sum_{j=1}^M (\alpha \mathcal{U}_{1j} \sqrt{1-\eta} + \beta_j \sqrt{\eta}) a_j^\dagger} |\text{VAC}\rangle \\ & \quad \times e^{-\frac{1}{\bar{n}} \sum_{j=1}^M |\beta_j|^2 - \sum_{j=1}^M |\alpha^* \mathcal{U}_{1j}^* \sqrt{1-\eta} + \beta_j^* \sqrt{\eta}|^2} \\ & \quad \times \langle\text{VAC}| e^{\sum_{j=1}^M (\alpha^* \mathcal{U}_{1j}^* \sqrt{1-\eta} + \beta_j^* \sqrt{\eta}) a_j^\dagger}. \end{aligned} \quad (\text{C2})$$

The final step is to apply the inverse unitary transformation

followed by $(M - 1)$ -mode vacuum measurements on the resulting state. The former leads to the operator exponent

$$\begin{aligned} & \sum_{j=1}^M (\alpha \mathcal{U}_{1j} \sqrt{1-\eta} + \beta_j \sqrt{\eta}) \sum_{k=1}^M \mathcal{U}_{jk}^\dagger a_k^\dagger \\ &= \left(\alpha \sqrt{1-\eta} + \sqrt{\eta} \sum_{j=1}^M \beta_j \mathcal{U}_{j1}^\dagger \right) a_1^\dagger + \sqrt{\eta} \sum_{j=1}^M \sum_{k=2}^M \beta_j \mathcal{U}_{jk}^\dagger a_k^\dagger. \end{aligned} \quad (\text{C3})$$

After the vacuum measurements, we arrive at the output state

$$\begin{aligned} \langle \alpha | \langle \alpha | \rangle_{\text{supp}} &\propto \int \frac{(d\beta)}{\bar{n}^M \pi^M} \left| \alpha \sqrt{1-\eta} + \sqrt{\eta} \sum_{j=1}^M \beta_j \mathcal{U}_{j1}^\dagger \right\rangle \\ &\times e^{-\frac{1}{\bar{n}} \sum_{j=1}^M |\beta_j|^2} f(\alpha, \beta; \eta, \mathcal{U}) \left\langle \alpha \sqrt{1-\eta} + \sqrt{\eta} \sum_{j=1}^M \beta_j \mathcal{U}_{j1}^\dagger \right\rangle, \end{aligned} \quad (\text{C4})$$

where in terms of the computational basis,

$$\begin{aligned} \log f(\alpha, \beta; \eta, \mathcal{U}) &= - \sum_{j=1}^M \left| \alpha \mathcal{U}_{1j} \sqrt{1-\eta} + \beta_j \sqrt{\eta} \right|^2 \\ &+ \left| \alpha \sqrt{1-\eta} + \sqrt{\eta} \sum_{j=1}^M \beta_j \mathcal{U}_{j1}^\dagger \right|^2 \\ &= -\eta \sum_{j=1}^M |\beta_j|^2 + \eta \sum_{j=1}^M \sum_{k=1}^M \beta_j \beta_k^* \mathcal{U}_{j1}^\dagger \mathcal{U}_{1k} \\ &= -\eta \beta^\dagger (\mathbf{1} - \mathcal{U}^\top \mathbf{e} \mathbf{e}^\top \mathcal{U}^*) \beta \end{aligned} \quad (\text{C5})$$

and $\mathbf{e} = (1 \ 0 \ \dots \ 0)^\top$.

To proceed, one can perform the variable change $\beta' \equiv \mathcal{U}^* \beta$ of unit Jacobian, so that we may rewrite

$$\begin{aligned} \langle \alpha | \langle \alpha | \rangle_{\text{supp}} &\propto \int \frac{(d\beta')}{\bar{n}^M \pi^M} \left| \alpha \sqrt{1-\eta} + \sqrt{\eta} \beta'_1 \right\rangle \\ &\times e^{-\frac{1}{\bar{n}} \sum_{j=1}^M |\beta'_j|^2 - \eta \beta'^\dagger (\mathbf{1} - \mathbf{e} \mathbf{e}^\top) \beta'} \left\langle \alpha \sqrt{1-\eta} + \sqrt{\eta} \beta'_1 \right\rangle, \end{aligned} \quad (\text{C6})$$

where we now see that

$$\eta \beta'^\dagger (\mathbf{1} - \mathbf{e} \mathbf{e}^\top) \beta' = \eta \sum_{j=2}^M |\beta'_j|^2. \quad (\text{C7})$$

This observation helps take care of $M - 1$ integrals, which themselves give the vacuum-measurement success rate

$$p_{\text{succ}} = \left(\int \frac{(d\beta')}{\bar{n} \pi} e^{-\left(\frac{1}{\bar{n}} + \eta\right) |\beta'|^2} \right)^{M-1} = \left(\frac{1}{1 + \bar{n} \eta} \right)^{M-1}, \quad (\text{C8})$$

and produces the suppressed state as

$$\begin{aligned} \langle \alpha | \langle \alpha | \rangle_{\text{supp}} &= \int \frac{(d\beta'_1)}{\bar{n} \pi} \left| \alpha \sqrt{1-\eta} + \sqrt{\eta} \beta'_1 \right\rangle e^{-\frac{1}{\bar{n}} |\beta'_1|^2} \\ &\times \left\langle \alpha \sqrt{1-\eta} + \sqrt{\eta} \beta'_1 \right\rangle. \end{aligned} \quad (\text{C9})$$

Therefore, the M -mode VMZ protocol leaves the thermally-noisy state intact. As this fails for the coherent state, we conclude likewise for *any* state ρ .

A similar calculation with RDN yields the suppressed coherent state of a (expectedly) very similar form:

$$\begin{aligned} \langle \alpha | \langle \alpha | \rangle_{\text{supp}} &\propto \int (d\beta) p(\beta_1, \beta_1^*) \dots p(\beta_M, \beta_M^*) \left| \alpha + \sum_{j=1}^M \beta_j \mathcal{U}_{j1}^\dagger \right\rangle \\ &\times e^{-\beta^\dagger (\mathbf{1} - \mathcal{U}^\top \mathbf{e} \mathbf{e}^\top \mathcal{U}^*) \beta} \left\langle \alpha + \sum_{j=1}^M \beta_j \mathcal{U}_{j1}^\dagger \right\rangle. \end{aligned} \quad (\text{C10})$$

Hence, the same variable change would result in

$$\begin{aligned} \langle \alpha | \langle \alpha | \rangle_{\text{supp}} &\propto \int (d\beta') p((\mathcal{U}^\top \beta')_1, (\mathcal{U}^\top \beta')_1^*) \dots p((\mathcal{U}^\top \beta')_M, (\mathcal{U}^\top \beta')_M^*) \\ &\times |\alpha + \beta'_1\rangle e^{-\sum_{j=2}^M |\beta'_j|^2} \langle \alpha + \beta'_1|. \end{aligned} \quad (\text{C11})$$

If $p(\beta, \beta^*) = e^{-|\beta|^2/\sigma^2}/(\pi\sigma^2)$, that is for a GDN channel, we realize that the output after the VMZ protocol is

$$\langle \alpha | \langle \alpha | \rangle_{\text{supp}} = \int (d\beta'_1) |\alpha + \beta'_1\rangle \frac{e^{-\frac{|\beta'_1|^2}{\sigma^2}}}{\pi\sigma^2} \langle \alpha + \beta'_1|, \quad (\text{C12})$$

which is just the original GDN-corrupted state.

Appendix D: Mutual compatibility between PSG-PEC mitigation and VMZ-suppression schemes

The purpose is to show the equivalence between Figs. 12(a) and (b), that is, the order in which an input state is treated with the PSG error-mitigation and M -mode VMZ error-suppression protocols is irrelevant. It is enough to look at the combined operations before the noise channel. Those after behave exactly the same way by symmetry. We adopt the usual trick of inspecting the action of these operations on the coherent state and generalize the result to all quantum states.

In Fig. 12(a), we swiftly find that the M -mode state right after U_M , the evolution operator of \mathcal{U} ,

$$\begin{aligned} \rho_{(a)} &= U_M |g \alpha\rangle \langle g \alpha| \otimes (|\text{vac}\rangle \langle \text{vac}|)^{\otimes M-1} U_M^\dagger \\ &= e^{g \alpha \sum_{j=1}^M \mathcal{U}_{1j} a_j^\dagger} |\text{vac}\rangle \langle \text{vac}| e^{-|g \alpha|^2} \langle \text{vac}| e^{g \alpha^* \sum_{j'=1}^M \mathcal{U}_{1j'}^* a_{j'}} \\ &= |g \alpha \mathcal{U}_{11}, \dots, g \alpha \mathcal{U}_{1M}\rangle \langle g \alpha \mathcal{U}_{11}, \dots, g \alpha \mathcal{U}_{1M}|. \end{aligned} \quad (\text{D1})$$

TABLE II. Values of c_{kn} rounded off to two decimal places, with the vanishingly-small values for $n > 6$ neglected. Actual values all sum to unity as they should.

c_{kn}	$n = 0$	$n = 1$	$n = 2$	$n = 3$	$n = 4$	$n = 5$	$n = 6$
$k = 1$	-1.30	-0.44	0.05	-0.00	-0.00	0.00	0.00
$k = 2$	6.93	1.43	-0.01	-0.00	-0.00	-0.00	0.00
$k = 3$	-2.87	0.59	0.18	-0.05	0.01	0.00	0.00
$k = 4$	-0.25	0.22	0.06	-0.02	0.00	0.00	0.00
$k = 5$	-1.19	-0.01	0.09	-0.02	0.00	-0.00	0.00
$k = 6$	2.43	-1.51	-0.68	0.09	-0.01	-0.01	-0.00
$k = 7$	-5.57	-0.29	0.04	-0.01	0.00	-0.00	0.00
$k = 8$	1.36	1.74	-0.02	0.03	-0.00	0.00	-0.00

For the circuit in Fig. 12(b), because $g^{a_1^\dagger a_1 + \dots + a_M^\dagger a_M}$ commutes with any BS, the M -mode state right after the PSGs is

$$\begin{aligned} \rho_{(b)} &= \sum_{k_1, \dots, k_M=0}^{\infty} \frac{(-1 + g^{-2})^{k_1 + \dots + k_M}}{k_1! \dots k_M!} \prod_{j=1}^M a_j^{k_j} W \prod_{j'=1}^M a_{j'}^{\dagger k_{j'}}, \\ W &= U_M |g\alpha\rangle e^{(g^2 - 1)|\alpha|^2} \langle g\alpha| \otimes (|\text{VAC}\rangle \langle \text{VAC}|)^{\otimes M-1} U_M^\dagger \\ &= U_M e^{g\alpha a_1^\dagger} |\text{VAC}\rangle e^{-|\alpha|^2} \langle \text{VAC}| e^{g\alpha^* a_1} U_M^\dagger \\ &= e^{g\alpha \sum_{j=1}^M \mathcal{U}_{1j} a_j^\dagger} |\text{VAC}\rangle e^{-|\alpha|^2} \langle \text{VAC}| e^{g\alpha^* \sum_{j'=1}^M \mathcal{U}_{1j'} a_{j'}}, \end{aligned} \quad (\text{D2})$$

such that

$$\begin{aligned} \prod_{j=1}^M a_j^{k_j} W \prod_{j'=1}^M a_{j'}^{\dagger k_{j'}} &= |g\alpha \mathcal{U}_{11}, \dots, g\alpha \mathcal{U}_{1M}\rangle e^{(g^2 - 1)|\alpha|^2} \\ &\times |g\alpha \mathcal{U}_{11}|^{2k_1} \dots |g\alpha \mathcal{U}_{1M}|^{2k_M} \langle g\alpha \mathcal{U}_{11}, \dots, g\alpha \mathcal{U}_{1M}|. \end{aligned} \quad (\text{D3})$$

As the multiple sums simplify to

$$\begin{aligned} &\prod_{j=1}^M \sum_{k_j=0}^{\infty} \frac{(-1 + g^{-2})^{k_j}}{k_j!} |g\alpha \mathcal{U}_{1j}|^{2k_j} \\ &= \prod_{j=1}^M e^{|g\alpha|^2 |\mathcal{U}_{1j}|^2 (-1 + g^{-2})} = e^{-|\alpha|^2 (g^2 - 1)}, \end{aligned} \quad (\text{D4})$$

we find that $\rho_{(a)} = \rho_{(b)}$.

Appendix E: Miscellaneous

1. Squeezed displaced-Fock representation for the squeezed-“cat” code in Sec. IID

Since displaced Fock states span the entire phase space (for example, in the manner of Wigner operators [139]),

we can write any operator as their linear combination inasmuch as Eq. (12). As the bosonic code of interest here is the squeezed-“cat” code, we can apply the same amount of squeezing to these displaced Fock projectors. Given that $O = |\text{enc. in}\rangle \langle \text{enc. in}|$, the objective is to find $\{\beta_k\}$ and $\{c_{kn}\}$ by

Algorithm 2 Optimizing squeezed displaced-Fock meas.

- 1: Specify the dimension d of the truncated Hilbert space, number of squeezed displaced-Fock bases K and a small $\epsilon > 0$.
- 2: Set termination flag `flag` to 0.
- 3: Define $\mathcal{F}_{\beta, \mathbf{c}} = \sum_{k=1}^K \sum_{n=0}^{d-1} c_{kn} |\langle \text{enc. in} | S(z) D(\beta_k) | n \rangle|^2$.
- 4: Start with a random β and $c_{kn} = 1$.
- 5: **while** `flag = 0` **do**
- 6: Maximize $\mathcal{F}_{\beta, \mathbf{c}}$ over β whilst fixing \mathbf{c} .
- 7: Set β as the new optimized column.
- 8: Maximize $\mathcal{F}_{\beta, \mathbf{c}}$ over \mathbf{c} whilst fixing β , subject to
- 9: $\sum_{k=1}^K \sum_{n=0}^{d-1} c_{kn} = 1$ and
- 10: $\sum_{k=1}^K \sum_{n=0}^{d-1} S(z) D(\beta_k) | n \rangle c_{kn} \langle n | D(\beta_k)^\dagger S(z)^\dagger \geq 0$.
- 11: Set \mathbf{c} as the new optimized matrix.
- 12: **if** $\mathcal{F}_{\beta, \mathbf{c}} > 1 - \epsilon$ **then**
- 13: Set `flag = 1`.
- 14: **end if**
- 15: **end while**

Lines 8 to 10 form a semidefinite program that can be efficiently executed using packages such as CVX [140–142]. Algorithm 2 generalizes a procedure in [143]. For $z = 3\text{dB}$ and $\alpha = 1$, Alg. 2 yields the set of $K = 8$ amplitudes $\{-0.1721 + 0.3930i, 0.4398 + 0.1135i, 0.3325 - 0.0789i, 0.2340 + 0.3229i, 0.0777 - 0.2548i, 0.2100 + 0.0366i, 0.4174 + 0.2144i, 0.1963 + 0.1448i\}$ and the c_{kn} s that gave an optimized $\mathcal{F}_{\beta, \mathbf{c}} > 0.99$ are given in Tab. II. The 64 squeezed displaced-Fock projectors that specify $|\text{enc. in}\rangle \langle \text{enc. in}|$ consist of 56 pure projectors $S(z) D(\beta_k) | n \rangle \langle n | D(\beta_k)^\dagger S(z)^\dagger$ for $0 \leq n \leq 6$, $1 \leq k \leq 8$ and 8 mixed projectors $1 - \sum_{n=0}^6 S(z) D(\beta_k) | n \rangle \langle n | D(\beta_k)^\dagger S(z)^\dagger$ for $1 \leq k \leq 8$.

2. Short proof of inequality (19)

Since $s_l = \lambda_\gamma \delta_{l,1}$ and $\overline{e^{i(\phi_j - \phi_{j'})}} = |\lambda_\gamma|^2$ if $j \neq j'$,

$$\begin{aligned} &|s_l - \overline{s_l}|^2 = |s_l|^2 - |\lambda_\gamma|^2 \delta_{l,1} \\ &= \sum_{j=1}^M |\mathcal{U}_{j1}|^2 |\mathcal{U}_{jl}|^2 + |\lambda_\gamma|^2 \underbrace{\sum_{j \neq j'}^M \mathcal{U}_{lj}^\dagger \mathcal{U}_{j1} \mathcal{U}_{lj'}^\dagger \mathcal{U}_{j'l}}_{= \delta_{l,1} - \sum_{j=1}^M |\mathcal{U}_{j1}|^2 |\mathcal{U}_{jl}|^2} \\ &= (1 - |\lambda_\gamma|^2) \sum_{j=1}^M |\mathcal{U}_{j1}|^2 |\mathcal{U}_{jl}|^2, \end{aligned} \quad (\text{E1})$$

and all else follows from the basic Chebyshev inequality.

3. Averaging over unitary two-designs

If \mathcal{U} is an M -dimensional unitary two-design (TD), which encompasses the Haar-random unitary operators, given M -dimensional \mathcal{A} , \mathcal{B} , \mathcal{C} and \mathcal{Y} , and M^2 -dimensional \mathcal{Z} , the following identities are well-known [116, 118, 119, 144, 145]:

$$\overline{\mathcal{U}\mathcal{Y}\mathcal{U}^\dagger}^{\text{TD}} = \frac{\text{tr}\{\mathcal{Y}\}}{M}, \quad (\text{E2})$$

$$\begin{aligned} \overline{\mathcal{U}^{\otimes 2}\mathcal{Z}\mathcal{U}^{\dagger\otimes 2}}^{\text{TD}} &= \left[\frac{\text{tr}\{\mathcal{Z}\}}{M^2-1} - \frac{\text{tr}\{\mathcal{Z}\tau\}}{M(M^2-1)} \right] \mathbf{1} \\ &+ \left[\frac{\text{tr}\{\mathcal{Z}\tau\}}{M^2-1} - \frac{\text{tr}\{\mathcal{Z}\}}{M(M^2-1)} \right] \tau, \end{aligned} \quad (\text{E3})$$

$$\begin{aligned} \overline{\mathcal{U}\mathcal{A}\mathcal{U}^\dagger\mathcal{B}\mathcal{U}\mathcal{C}\mathcal{U}^\dagger}^{\text{TD}} &= \frac{\text{tr}\{\mathcal{A}\}\text{tr}\{\mathcal{C}\}\mathcal{B} + \text{tr}\{\mathcal{B}\}\text{tr}\{\mathcal{A}\mathcal{C}\}\mathbf{1}}{M^2-1} \\ &- \frac{\text{tr}\{\mathcal{A}\}\text{tr}\{\mathcal{B}\}\text{tr}\{\mathcal{C}\}\mathbf{1} + \text{tr}\{\mathcal{A}\mathcal{C}\}\mathcal{B}}{M(M^2-1)}, \end{aligned} \quad (\text{E4})$$

where τ is the swap operator. Using (E4) and the substitutions $\mathcal{A} = |k\rangle\langle k|$, $\mathcal{B} = |j\rangle\langle j|$ and $\mathcal{C} = |l\rangle\langle l|$, the two-design average

$$\begin{aligned} &\sum_{j=1}^M \overline{\mathcal{U}|k\rangle\langle k|\mathcal{U}^\dagger|j\rangle\langle j|\mathcal{U}|l\rangle\langle l|\mathcal{U}^\dagger}^{\text{TD}} \\ &= \frac{1}{M^2-1} (|j\rangle\langle j| + \delta_{k,l}\mathbf{1}) - \frac{1}{M(M^2-1)} (1 + |j\rangle\langle j| \delta_{k,l}) \end{aligned} \quad (\text{E5})$$

straightforwardly yields

$$\sum_{j=1}^M |\mathcal{U}_{jk}|^2 |\mathcal{U}_{jl}|^2 = \frac{1 + \delta_{k,l}}{M+1}. \quad (\text{E6})$$

4. Approximating S_{mn} for central-Gaussian dephasing channels

If $p_j = |\mathcal{U}_{j1}|^2$, where clearly $\sum_{j=1}^M p_j = 1$, then $s_1 = \sum_{j=1}^M p_j e^{i\phi_j}$ and the average over the central-Gaussian distribution *exactly* gives

$$\begin{aligned} S_{mn} &= \overline{s_1^m s_1^{*n}} \\ &= \sum_{\mathbf{k}, \mathbf{k}'} \frac{m!}{k_1! \dots k_M!} \frac{n!}{k'_1! \dots k'_M!} p_1^{k_1+k'_1} \dots p_M^{k_M+k'_M} \\ &\quad \times e^{-\frac{\gamma}{2}(k_1-k'_1)^2 - \dots - \frac{\gamma}{2}(k_M-k'_M)^2}, \end{aligned} \quad (\text{E7})$$

where it is understood that the summations respect the constraints $\sum_{j=1}^M k_j = m$ and $\sum_{j=1}^M k'_j = n$. This is followed by a Taylor expansion of the exponential function $e^{-\frac{\gamma}{2}(k_j-k'_j)^2} \cong 1 - \frac{\gamma}{2}(k_j-k'_j)^2$ up to first order in γ . Since the right-hand side of (E7) is just averages over two multinomial distributions that are both defined by p_j , up to $\mathcal{O}(\gamma)$,

$$\begin{aligned} S_{mn} &\cong 1 - \frac{\gamma}{2} \sum_{j=1}^M \mathbb{E}[(k_j - k'_j)^2] \\ &= 1 - \frac{\gamma}{2} \sum_{j=1}^M \left[(m+n)(p_j - p_j^2) + (mp_j)^2 + (np_j)^2 \right. \\ &\quad \left. - 2mnp_j^2 \right] \\ &= 1 - \frac{\gamma}{2} [(m+n)w + (m-n)^2(1-w)]. \end{aligned} \quad (\text{E8})$$

For any γ , if $m, n \gg 1$, then one can apply the central limit theorem to multinomial distributions [120], which is summarized in Appendix E5 for completeness, such that

$$\begin{aligned} &\frac{m!}{k_1! \dots k_M!} \delta_{k_1+\dots+k_M, m} p_1^{k_1} p_2^{k_2} \dots p_M^{k_M} \\ &\cong \frac{e^{-\frac{1}{2}(\tilde{\mathbf{x}} - m\tilde{\mathbf{p}}) \cdot \Sigma_m^{-1} \cdot (\tilde{\mathbf{x}} - m\tilde{\mathbf{p}})}}{\sqrt{(2\pi)^{M-1} \det\{\Sigma_m\}}}, \end{aligned} \quad (\text{E9})$$

where $\tilde{\mathbf{x}} = (k_1 \ k_2 \ \dots \ k_{M-1})^\top$,

$$\Sigma_m = m(\tilde{\mathbf{P}} - \tilde{\mathbf{p}}\tilde{\mathbf{p}}^\top), \quad \det\{\Sigma_m\} = m^{M-1} p_1 p_2 \dots p_M \quad (\text{E10})$$

and the $(M-1)$ -dimensional matrices are defined as

$$\tilde{\mathbf{P}} = \begin{pmatrix} p_1 & 0 & \dots & 0 \\ 0 & p_2 & \dots & 0 \\ \vdots & \vdots & \ddots & \vdots \\ 0 & 0 & \dots & p_{M-1} \end{pmatrix}, \quad \tilde{\mathbf{p}} = \begin{pmatrix} p_1 \\ p_2 \\ \vdots \\ p_{M-1} \end{pmatrix}, \quad \mathbf{1} = \begin{pmatrix} 1 \\ 1 \\ \vdots \\ 1 \end{pmatrix}. \quad (\text{E11})$$

Using this familiar approximation,

$$\begin{aligned} &\mathbb{E} \left[e^{-\frac{\gamma}{2} \sum_j (k_j - k'_j)^2} \right] \\ &\cong \int (d\tilde{\mathbf{x}}) \frac{e^{-\frac{1}{2}(\tilde{\mathbf{x}} - m\tilde{\mathbf{p}}) \cdot \Sigma_m^{-1} \cdot (\tilde{\mathbf{x}} - m\tilde{\mathbf{p}})}}{\sqrt{(2\pi)^{M-1} \det\{\Sigma_m\}}} \\ &\quad \times \int (d\tilde{\mathbf{x}}') \frac{e^{-\frac{1}{2}(\tilde{\mathbf{x}}' - n\tilde{\mathbf{p}}) \cdot \Sigma_n^{-1} \cdot (\tilde{\mathbf{x}}' - n\tilde{\mathbf{p}})}}{\sqrt{(2\pi)^{M-1} \det\{\Sigma_n\}}} e^{-\frac{\gamma}{2}(\tilde{\mathbf{x}}' - \tilde{\mathbf{x}})^2}. \end{aligned} \quad (\text{E12})$$

Using the standard result

$$\int (d\mathbf{x}) e^{-\mathbf{x} \cdot \mathbf{A} \cdot \mathbf{x} + \mathbf{b} \cdot \mathbf{x}} = \sqrt{\frac{\pi^D}{\det\{\mathbf{A}\}}} e^{\frac{1}{4}\mathbf{b} \cdot \mathbf{A}^{-1} \cdot \mathbf{b}} \quad (\text{E13})$$

for real D -dimensional $\mathbf{A} > 0$ and \mathbf{b} , with tenacity, one gets

$$S_{mn} = \frac{e^{-\frac{\gamma}{2}(m-n)^2 \sum_{j=1}^M p_j^2}}{2^{M-1} \sqrt{\det\{\Sigma_m\} \det\{\Sigma_n\} \det\{\mathbf{C}\}}} e^{\frac{1}{4}\mathbf{b} \cdot \mathbf{C}^{-1} \cdot \mathbf{b}} \quad (\text{E14})$$

that holds for any $\tilde{\mathbf{p}}$, where $\mathbf{B} = (\gamma/2)(\mathbf{1} + \mathbf{1}\mathbf{1}^\top)$,

$$\mathbf{C} = \begin{pmatrix} \frac{1}{2}\Sigma_m^{-1} + \mathbf{B} & -\mathbf{B} \\ -\mathbf{B} & \frac{1}{2}\Sigma_n^{-1} + \mathbf{B} \end{pmatrix}, \mathbf{b} = \gamma(m-n) \begin{pmatrix} p_M \mathbf{1} - \tilde{\mathbf{p}} \\ \tilde{\mathbf{p}} - p_M \mathbf{1} \end{pmatrix}. \quad (\text{E15})$$

Some more acrobatics turn the determinant triple product into

$$\begin{aligned} & \det\{\Sigma_m\} \det\{\Sigma_n\} \det\{\mathbf{C}\} \\ &= \det \left\{ \begin{pmatrix} \frac{1}{2}\mathbf{1} + \Sigma_m \mathbf{B} & -\Sigma_m \mathbf{B} \\ -\Sigma_n \mathbf{B} & \frac{1}{2}\mathbf{1} + \Sigma_n \mathbf{B} \end{pmatrix} \right\} \\ &= \det \left\{ \left(\frac{1}{2}\mathbf{1} + \Sigma_m \mathbf{B} \right) \left(\frac{1}{2}\mathbf{1} + \Sigma_n \mathbf{B} \right) - \Sigma_m \mathbf{B} \Sigma_n \mathbf{B} \right\} \\ &= \det \left\{ \frac{1}{4}\mathbf{1} + \frac{1}{2}(\Sigma_m + \Sigma_n) \mathbf{B} \right\}, \quad (\text{E16}) \end{aligned}$$

where we note that $\Sigma_m \mathbf{B}$ commutes with $\Sigma_n \mathbf{B}$ and that for

$$\Gamma = \begin{pmatrix} \mathbf{A} & \mathbf{B} \\ \mathbf{C} & \mathbf{D} \end{pmatrix} \text{ with an invertible } \mathbf{A}, \quad (\text{E17})$$

the identity $\det\{\Gamma\} = \det\{\mathbf{A}\} \det\{\mathbf{D} - \mathbf{C}\mathbf{A}^{-1}\mathbf{B}\}$ holds.

For a Hadamard \mathcal{U} ,

$$\begin{aligned} \Sigma_m &= \frac{m}{M} \left(\mathbf{1} - \frac{1}{M} \mathbf{1}\mathbf{1}^\top \right), \mathbf{b} = \mathbf{0} \\ \Sigma_m \mathbf{B} &= \frac{\gamma m}{2M} \left(\mathbf{1} - \frac{1}{M} \mathbf{1}\mathbf{1}^\top \right) (\mathbf{1} + \mathbf{1}\mathbf{1}^\top) = \frac{\gamma m}{2M} \mathbf{1}, \\ \det \left\{ \frac{1}{4}\mathbf{1} + \frac{1}{2}(\Sigma_m + \Sigma_n) \mathbf{B} \right\} &= \left[\frac{1 + \frac{\gamma}{M}(m+n)}{4} \right]^{M-1}, \quad (\text{E18}) \end{aligned}$$

leading to (24). Based on numerical evidence, for finite M , Eq. (24) is also rather accurate even for small m and n .

5. Approximating a multinomial distribution

The M -mode multinomial distribution characterized by $n > 0$, $\tilde{\mathbf{p}} = (p_1 p_2 \dots p_{M-1})^\top$ and $p_M = 1 - p_1 - p_2 - \dots - p_{M-1}$,

$$\text{pr}(n, \tilde{\mathbf{p}}) = \frac{n!}{k_1! k_2! \dots k_M!} \delta_{k_1 + \dots + k_M, n} p_1^{k_1} p_2^{k_2} \dots p_M^{k_M}, \quad (\text{E19})$$

can be very well approximated using the Stirling formula $k! \cong k^k e^{-k} \sqrt{2\pi k}$, which works extremely well even for a very small k . Together with the definitions $\nu_j = k_j/n$, $y = 1 - \sum_{j=1}^{M-1} \nu_j$ and the crucial recognition that there are

only $M - 1$ independent p_j s and ν_j s,

$$\begin{aligned} & \log \text{pr}(n, \tilde{\mathbf{p}}) \\ & \cong -\log \sqrt{(2\pi n)^{M-1}} - \sum_{j=1}^{M-1} \left(n \nu_j \log \nu_j + \frac{1}{2} \log \nu_j \right) \\ & \quad + n \sum_{j=1}^{M-1} \nu_j \log p_j + n y \log p_M - \left(n y \log y + \frac{1}{2} \log y \right). \quad (\text{E20}) \end{aligned}$$

A standard approach is to consider the situation in which $\nu_j \cong p_j$ for a sufficiently large n . One may then expand the constituents of $\log \text{pr}(n, \tilde{\mathbf{p}})$ to second order in $\nu_j - p_j$ for $1 \leq j \leq M - 1$, for which we acquire the first-order derivatives

$$\begin{aligned} \partial_{\nu_k} \left(\sum_{j=1}^{M-1} \log \nu_j + \log y \right) &= \frac{1}{\nu_k} - \frac{1}{y}, \\ \partial_{\nu_k} \left(\sum_{j=1}^{M-1} \nu_j \log \nu_j + y \log y \right) &= \log \nu_k - \log y, \quad (\text{E21}) \end{aligned}$$

and also the second-order derivatives (Hessian elements)

$$\begin{aligned} \partial_{\nu_l} \partial_{\nu_k} \left[\sum_{j=1}^{M-1} \log \nu_j + \log y \right] &= -\frac{\delta_{k,l}}{\nu_k^2} - \frac{1}{y^2}, \\ \partial_{\nu_l} \partial_{\nu_k} \left[\sum_{j=1}^{M-1} \nu_j \log \nu_j + y \log y \right] &= \frac{\delta_{k,l}}{\nu_k} + \frac{1}{y}. \quad (\text{E22}) \end{aligned}$$

With these, after keeping only terms of $\mathcal{O}(n)$ and $-(1/2) \sum_{j=1}^M \log p_j$ for consistent $\text{pr}(n, \tilde{\mathbf{p}})$ normalization,

$$\begin{aligned} & -\sum_{j=1}^{M-1} \left(n \nu_j \log \nu_j + \frac{1}{2} \log \nu_j \right) - \left(n y \log y + \frac{1}{2} \log y \right) \\ & \cong -\frac{1}{2} \sum_{j=1}^M \log p_j - n \sum_{j=1}^{M-1} \nu_j \log p_j - n y \log p_M \\ & \quad - \frac{n^2}{2} (\tilde{\mathbf{v}} - \tilde{\mathbf{p}}) \cdot \Sigma_n^{-1} \cdot (\tilde{\mathbf{v}} - \tilde{\mathbf{p}}), \quad (\text{E23}) \end{aligned}$$

where

$$\Sigma_n^{-1} = \frac{1}{n} \left(\tilde{\mathbf{P}}^{-1} + \frac{\mathbf{1}\mathbf{1}^\top}{p_M} \right) = \left[n(\tilde{\mathbf{P}} - \tilde{\mathbf{p}}\tilde{\mathbf{p}}^\top) \right]^{-1} \quad (\text{E24})$$

and both $\tilde{\mathbf{P}}$ and $\tilde{\mathbf{p}}$ are the $(M - 1)$ -dimensional objects as defined in (E11). Hereafter, exponentiating the approximated right-hand side of (E20) nabs us (E9).

- [1] P. T. Cochrane, G. J. Milburn, and W. J. Munro, Macroscopically distinct quantum-superposition states as a bosonic code for amplitude damping, *Phys. Rev. A* **59**, 2631 (1999).
- [2] D. Gottesman, A. Kitaev, and J. Preskill, Encoding a qubit in an oscillator, *Phys. Rev. A* **64**, 012310 (2001).
- [3] M. H. Michael, M. Silveri, R. T. Brierley, V. V. Albert, J. Salmilehto, L. Jiang, and S. M. Girvin, New class of quantum error-correcting codes for a bosonic mode, *Phys. Rev. X* **6**, 031006 (2016).
- [4] V. V. Albert, K. Noh, K. Duivenvoorden, D. J. Young, R. T. Brierley, P. Reinhold, C. Vuillot, L. Li, C. Shen, S. M. Girvin, B. M. Terhal, and L. Jiang, Performance and structure of single-mode bosonic codes, *Phys. Rev. A* **97**, 032346 (2018).
- [5] K. Jacobs, A. N. Jordan, and E. K. Irish, Energy measurements and preparation of canonical phase states of a nanomechanical resonator, *Europhysics Letters* **82**, 18003 (2008).
- [6] H. M. Vasconcelos, L. Sanz, and S. Glancy, All-optical generation of states for “Encoding a qubit in an oscillator”, *Opt. Lett.* **35**, 3261 (2010).
- [7] Z. Leghtas, G. Kirchmair, B. Vlastakis, R. J. Schoelkopf, M. H. Devoret, and M. Mirrahimi, Hardware-efficient autonomous quantum memory protection, *Phys. Rev. Lett.* **111**, 120501 (2013).
- [8] M. Mirrahimi, Z. Leghtas, V. V. Albert, S. Touzard, R. J. Schoelkopf, L. Jiang, and M. H. Devoret, Dynamically protected cat-qubits: a new paradigm for universal quantum computation, *New Journal of Physics* **16**, 045014 (2014).
- [9] M. Eaton, R. Nehra, and O. Pfister, Non-gaussian and Gottesman–Kitaev–Preskill state preparation by photon catalysis, *New Journal of Physics* **21**, 113034 (2019).
- [10] W.-L. Ma, S. Puri, R. J. Schoelkopf, M. H. Devoret, S. Girvin, and L. Jiang, Quantum control of bosonic modes with superconducting circuits, *Science Bulletin* **66**, 1789 (2021).
- [11] J. Hastrup, K. Park, J. B. Brask, R. Filip, and U. L. Andersen, Measurement-free preparation of grid states, *npj Quantum Information* **7**, 17 (2021).
- [12] K. Fukui, M. Endo, W. Asavanant, A. Sakaguchi, J.-i. Yoshikawa, and A. Furusawa, Generating the Gottesman–Kitaev–Preskill qubit using a cross-Kerr interaction between squeezed light and Fock states in optics, *Phys. Rev. A* **105**, 022436 (2022).
- [13] R. Dahan, G. Baranes, A. Gorlach, R. Ruimy, N. Rivera, and I. Kaminer, Creation of optical cat and gkp states using shaped free electrons, *Phys. Rev. X* **13**, 031001 (2023).
- [14] S. Konno, W. Asavanant, F. Hanamura, H. Nagayoshi, K. Fukui, A. Sakaguchi, R. Ide, F. China, M. Yabuno, S. Miki, H. Terai, K. Takase, M. Endo, P. Marek, R. Filip, P. van Loock, and A. Furusawa, Logical states for fault-tolerant quantum computation with propagating light, *Science* **383**, 289 (2024).
- [15] K. Takase, F. Hanamura, H. Nagayoshi, J. E. Bourassa, R. N. Alexander, A. Kawasaki, W. Asavanant, M. Endo, and A. Furusawa, Generation of flying logical qubits using generalized photon subtraction with adaptive Gaussian operations, *Phys. Rev. A* **110**, 012436 (2024).
- [16] A. P. Lund, H. Jeong, T. C. Ralph, and M. S. Kim, Conditional production of superpositions of coherent states with inefficient photon detection, *Phys. Rev. A* **70**, 020101 (2004).
- [17] H. Jeong, M. S. Kim, T. C. Ralph, and B. S. Ham, Generation of macroscopic superposition states with small nonlinearity, *Phys. Rev. A* **70**, 061801 (2004).
- [18] A. Ourjoumtsev, H. Jeong, R. Tualle-Brouiri, and P. Grangier, Generation of optical ‘Schrödinger cats’ from photon number states, *Nature* **448**, 784 (2007).
- [19] U. Andersen, G. Leuchs, and C. Silberhorn, Continuous-variable quantum information processing, *Laser & Photonics Reviews* **4**, 337.
- [20] A. Mari, V. Giovannetti, and A. S. Holevo, Quantum state majorization at the output of bosonic Gaussian channels, *Nature Communications* **5**, 3826 (2014).
- [21] A. Joshi, K. Noh, and Y. Y. Gao, Quantum information processing with bosonic qubits in circuit QED, *Quantum Science and Technology* **6**, 033001 (2021).
- [22] A. Anteneh and O. Pfister, Sample efficient graph classification using binary Gaussian boson sampling, *Phys. Rev. A* **108**, 062411 (2023).
- [23] T. C. Ralph, A. Gilchrist, G. J. Milburn, W. J. Munro, and S. Glancy, Quantum computation with optical coherent states, *Phys. Rev. A* **68**, 042319 (2003).
- [24] P. Aliferis, F. Brito, D. P. DiVincenzo, J. Preskill, M. Steffen, and B. M. Terhal, Fault-tolerant computing with biased-noise superconducting qubits: a case study, *New J. Phys.* **11**, 013061 (2009).
- [25] K. Noh, V. V. Albert, and L. Jiang, Quantum capacity bounds of Gaussian thermal loss channels and achievable rates with Gottesman–Kitaev–Preskill codes, *IEEE Transactions on Information Theory* **65**, 2563 (2019).
- [26] A. L. Grimsmo, J. Combes, and B. Q. Baragiola, Quantum computing with rotation-symmetric bosonic codes, *Phys. Rev. X* **10**, 011058 (2020).
- [27] S. Omkar, Y. S. Teo, and H. Jeong, Resource-efficient topological fault-tolerant quantum computation with hybrid entanglement of light, *Phys. Rev. Lett.* **125**, 060501 (2020).
- [28] L. S. Madsen, F. Laudenbach, M. F. Askarani, F. Rortais, T. Vincent, J. F. F. Bulmer, F. M. Miatto, L. Neuhaus, L. G. Helt, M. J. Collins, A. E. Lita, T. Gerrits, S. W. Nam, V. D. Vaidya, M. Menotti, I. Dhand, Z. Vernon, N. Quesada, and J. Lavoie, Quantum computational advantage with a programmable photonic processor, *Nature* **606**, 75 (2022).
- [29] Q. Xu, P. Zeng, D. Xu, and L. Jiang, Fault-tolerant operation of bosonic qubits with discrete-variable ancillae, *Phys. Rev. X* **14**, 031016 (2024).
- [30] C. Calcluth, N. Reichel, A. Ferraro, and G. Ferrini, Sufficient condition for universal quantum computation using bosonic circuits, *PRX Quantum* **5**, 020337 (2024).
- [31] J. Lee, N. Kang, S.-H. Lee, H. Jeong, L. Jiang, and S.-W. Lee, Fault-tolerant quantum computation by hybrid qubits with bosonic cat code and single photons, *PRX Quantum* **5**, 030322 (2024).
- [32] M.-A. Lemonde, D. Lachance-Quirion, G. Duclos-Cianci, N. E. Frattini, F. Hopfmueller, C. Gauvin-Ndiaye, J. Camirand-Lemyre, and P. St-Jean, Hardware-efficient fault-tolerant quantum computing with bosonic grid states in superconducting circuits (2024), [arXiv:2409.05813 \[quant-ph\]](https://arxiv.org/abs/2409.05813).
- [33] F. Caruso, J. Eisert, V. Giovannetti, and A. S. Holevo, Multi-mode bosonic Gaussian channels, *New Journal of Physics* **10**, 083030 (2008).
- [34] R. König and G. Smith, Classical capacity of quantum thermal noise channels to within 1.45 bits, *Phys. Rev. Lett.* **110**, 040501 (2013).
- [35] D. Suter and G. A. Álvarez, Colloquium: Protecting quantum information against environmental noise, *Rev. Mod. Phys.* **88**,

- 041001 (2016).
- [36] K. Noh, S. Pirandola, and L. Jiang, Enhanced energy-constrained quantum communication over bosonic gaussian channels, *Nature Communications* **11**, 457 (2020).
- [37] P. Leviant, Q. Xu, L. Jiang, and S. Rosenblum, Quantum capacity and codes for the bosonic loss-dephasing channel, *Quantum* **6**, 821 (2022).
- [38] K. Fukui, T. Matsuura, and N. C. Menicucci, Efficient concatenated bosonic code for additive gaussian noise, *Phys. Rev. Lett.* **131**, 170603 (2023).
- [39] Z. Huang, L. Lami, and M. M. Wilde, Exact quantum sensing limits for bosonic dephasing channels, *PRX Quantum* **5**, 020354 (2024).
- [40] S. Bose, J. Singh, A. Cabello, and H. Jeong, Long-distance entanglement sharing using hybrid states of discrete and continuous variables, *Phys. Rev. Appl.* **21**, 064013 (2024).
- [41] M. Bergmann and P. van Loock, Quantum error correction against photon loss using multicomponent cat states, *Phys. Rev. A* **94**, 042332 (2016).
- [42] S. Puri, A. Grimm, P. Campagne-Ibarcq, A. Eickbusch, K. Noh, G. Roberts, L. Jiang, M. Mirrahimi, M. H. Devoret, and S. M. Girvin, Stabilized cat in a driven nonlinear cavity: A fault-tolerant error syndrome detector, *Phys. Rev. X* **9**, 041009 (2019).
- [43] K. Noh and C. Chamberland, Fault-tolerant bosonic quantum error correction with the surface-gottesman-kitaev-preskill code, *Phys. Rev. A* **101**, 012316 (2020).
- [44] A. L. Grimsmo and S. Puri, Quantum error correction with the gottesman-kitaev-preskill code, *PRX Quantum* **2**, 10.1103/prxquantum.2.020101 (2021).
- [45] W. Cai, Y. Ma, W. Wang, C.-L. Zou, and L. Sun, Bosonic quantum error correction codes in superconducting quantum circuits, *Fundamental Research* **1**, 50 (2021).
- [46] J. Hastrup and U. L. Andersen, All-optical cat-code quantum error correction, *Phys. Rev. Res.* **4**, 043065 (2022).
- [47] A. J. Brady, A. Eickbusch, S. Singh, J. Wu, and Q. Zhuang, Advances in bosonic quantum error correction with gottesman-kitaev-preskill codes: Theory, engineering and applications, *Progress in Quantum Electronics* **93**, 100496 (2024).
- [48] F. Schmidt, D. Miller, and P. van Loock, Error-corrected quantum repeaters with gottesman-kitaev-preskill qudits, *Phys. Rev. A* **109**, 042427 (2024).
- [49] C. N. Gagatsos, B. A. Bash, S. Guha, and A. Datta, Bounding the quantum limits of precision for phase estimation with loss and thermal noise, *Phys. Rev. A* **96**, 062306 (2017).
- [50] X. Gao and L. Duan, Efficient classical simulation of noisy quantum computation (2018), [arXiv:1810.03176 \[quant-ph\]](https://arxiv.org/abs/1810.03176).
- [51] K. Noh, L. Jiang, and B. Fefferman, Efficient classical simulation of noisy random quantum circuits in one dimension, *Quantum* **4**, 318 (2020).
- [52] C. Oh, K. Noh, B. Fefferman, and L. Jiang, Classical simulation of lossy boson sampling using matrix product operators, *Phys. Rev. A* **104**, 022407 (2021).
- [53] C. Oh, Y. Lim, B. Fefferman, and L. Jiang, Classical simulation of boson sampling based on graph structure, *Phys. Rev. Lett.* **128**, 190501 (2022).
- [54] E. Fontana, M. S. Rudolph, R. Duncan, I. Rungger, and C. Cirstoiu, Classical simulations of noisy variational quantum circuits (2023), [arXiv:2306.05400 \[quant-ph\]](https://arxiv.org/abs/2306.05400).
- [55] M. Zhang, C. Wang, and Y. Han, Noisy random quantum circuit sampling and its classical simulation, *Advanced Quantum Technologies* **6**, 2300030.
- [56] L. Bugalho, E. Z. Cruzeiro, K. C. Chen, W. Dai, D. Englund, and Y. Omar, Resource-efficient simulation of noisy quantum circuits and application to network-enabled qram optimization, *npj Quantum Information* **9**, 105 (2023).
- [57] C. Oh, Classical simulability of constant-depth linear-optical circuits with noise (2024), [arXiv:2406.08086 \[quant-ph\]](https://arxiv.org/abs/2406.08086).
- [58] G. Bressanini, H. Kwon, and M. S. Kim, Gaussian boson sampling at finite temperature, *Phys. Rev. A* **109**, 013707 (2024).
- [59] N. Ofek, A. Petrenko, R. Heeres, P. Reinhold, Z. Leghtas, B. Vlastakis, Y. Liu, L. Frunzio, S. M. Girvin, L. Jiang, M. Mirrahimi, M. H. Devoret, and R. J. Schoelkopf, Extending the lifetime of a quantum bit with error correction in superconducting circuits, *Nature* **536**, 441 (2016).
- [60] J. Hastrup, J. S. Neergaard-Nielsen, and U. L. Andersen, Deterministic generation of a four-component optical cat state, *Opt. Lett.* **45**, 640 (2020).
- [61] D. Su, I. Dhand, and T. C. Ralph, Universal quantum computation with optical four-component cat qubits, *Phys. Rev. A* **106**, 042614 (2022).
- [62] M. Mičuda, I. Straka, M. Miková, M. Dušek, N. J. Cerf, J. Furašek, and M. Ježek, Noiseless loss suppression in quantum optical communication, *Phys. Rev. Lett.* **109**, 180503 (2012).
- [63] M. S. Winnel, N. Hosseinidehaj, and T. C. Ralph, Generalized quantum scissors for noiseless linear amplification, *Phys. Rev. A* **102**, 063715 (2020).
- [64] C. M. Nunn, J. D. Franson, and T. B. Pittman, Heralding on the detection of zero photons, *Phys. Rev. A* **104**, 033717 (2021).
- [65] S. U. Shringarpure, C. M. Nunn, T. B. Pittman, and J. D. Franson, Coherence of quantum states after noiseless attenuation, *Phys. Rev. A* **105**, 013704 (2022).
- [66] C. M. Nunn, J. D. Franson, and T. B. Pittman, Modifying quantum optical states by zero-photon subtraction, *Phys. Rev. A* **105**, 033702 (2022).
- [67] C. M. Nunn, S. U. Shringarpure, and T. B. Pittman, Transforming photon statistics through zero-photon subtraction, *Phys. Rev. A* **107**, 043711 (2023).
- [68] S. U. Shringarpure, Y. S. Teo, and H. Jeong, Error suppression in multicomponent cat codes with photon subtraction and teleamplification, *Opt. Express* **32**, 20719 (2024).
- [69] N. Gisin, N. Linden, S. Massar, and S. Popescu, Error filtration and entanglement purification for quantum communication, *Phys. Rev. A* **72**, 012338 (2005).
- [70] G. Lee, C. T. Hann, S. Puri, S. M. Girvin, and L. Jiang, Error suppression for arbitrary-size black box quantum operations, *Phys. Rev. Lett.* **131**, 190601 (2023).
- [71] Z. Liu, X. Zhang, Y.-Y. Fei, and Z. Cai, Virtual channel purification (2024), [arXiv:2402.07866 \[quant-ph\]](https://arxiv.org/abs/2402.07866).
- [72] Z. Cai, R. Babbush, S. C. Benjamin, S. Endo, W. J. Huggins, Y. Li, J. R. McClean, and T. E. O'Brien, Quantum error mitigation, *Rev. Mod. Phys.* **95**, 045005 (2023).
- [73] S. Endo, Y. Suzuki, K. Tsubouchi, R. Asaoka, K. Yamamoto, Y. Matsuzaki, and Y. Tokunaga, Quantum error mitigation for rotation symmetric bosonic codes with symmetry expansion (2022), [arXiv:2211.06164 \[quant-ph\]](https://arxiv.org/abs/2211.06164).
- [74] S. Endo, K. Anai, Y. Matsuzaki, Y. Tokunaga, and Y. Suzuki, Projective squeezing for translation symmetric bosonic codes (2024), [arXiv:2403.14218 \[quant-ph\]](https://arxiv.org/abs/2403.14218).
- [75] E. Knill, R. Laflamme, and G. J. Milburn, A scheme for efficient quantum computation with linear optics, *Nature* **409**, 46 (2001).
- [76] Y. Y. Gao, B. J. Lester, Y. Zhang, C. Wang, S. Rosenblum, L. Frunzio, L. Jiang, S. M. Girvin, and R. J. Schoelkopf, Programmable interference between two microwave quantum memories, *Phys. Rev. X* **8**, 021073 (2018).
- [77] C. S. Wang, J. C. Curtis, B. J. Lester, Y. Zhang, Y. Y. Gao, J. Freeze, V. S. Batista, P. H. Vaccaro, I. L. Chuang, L. Frunzio,

- L. Jiang, S. M. Girvin, and R. J. Schoelkopf, Efficient multi-photon sampling of molecular vibronic spectra on a superconducting bosonic processor, *Phys. Rev. X* **10**, 021060 (2020).
- [78] A. Taylor, G. Bressanini, H. Kwon, and M. S. Kim, Quantum error cancellation in photonic systems: Undoing photon losses, *Phys. Rev. A* **110**, 022622 (2024).
- [79] E. van den Berg, Z. K. Mineev, A. Kandala, and K. Temme, Probabilistic error cancellation with sparse pauli–lindblad models on noisy quantum processors, *Nature Physics* **19**, 1116 (2023).
- [80] R. S. Gupta, E. van den Berg, M. Takita, D. Ristè, K. Temme, and A. Kandala, Probabilistic error cancellation for dynamic quantum circuits, *Phys. Rev. A* **109**, 062617 (2024).
- [81] E. J. Anderson and B. A. Bash, Fundamental limits of thermal-noise lossy bosonic multiple access channel, in *2022 IEEE Globecom Workshops (GC Wkshps)* (2022) pp. 1–6.
- [82] C. Oh, S. Chen, Y. Wong, S. Zhou, H.-Y. Huang, J. A. H. Nielsen, Z.-H. Liu, J. S. Neergaard-Nielsen, U. L. Andersen, L. Jiang, and J. Preskill, Entanglement-enabled advantage for learning a bosonic random displacement channel (2024), [arXiv:2402.18809 \[quant-ph\]](https://arxiv.org/abs/2402.18809).
- [83] J. Schäfer, E. Karpov, and N. J. Cerf, Gaussian capacity of the quantum bosonic memory channel with additive correlated gaussian noise, *Phys. Rev. A* **84**, 032318 (2011).
- [84] K. Noh, S. M. Girvin, and L. Jiang, Encoding an oscillator into many oscillators, *Phys. Rev. Lett.* **125**, 080503 (2020).
- [85] F. A. Mele, F. Salek, V. Giovannetti, and L. Lami, Quantum communication on the bosonic loss-dephasing channel, *Phys. Rev. A* **110**, 012460 (2024).
- [86] A. Arqand, L. Memarzadeh, and S. Mancini, Energy-Constrained LOCC-Assisted Quantum Capacity of the Bosonic Dephasing Channel, *Entropy* **25** (2023).
- [87] M. Rexiti, L. Memarzadeh, and S. Mancini, Discrimination of dephasing channels, *Journal of Physics A: Mathematical and Theoretical* **55**, 245301 (2022).
- [88] Q. Zhuang, Quantum-enabled communication without a phase reference, *Phys. Rev. Lett.* **126**, 060502 (2021).
- [89] M. Fanizza, M. Rosati, M. Skotiniotis, J. Calsamiglia, and V. Giovannetti, Squeezing-enhanced communication without a phase reference, *Quantum* **5**, 608 (2021).
- [90] A. Arqand, L. Memarzadeh, and S. Mancini, Quantum capacity of a bosonic dephasing channel, *Phys. Rev. A* **102**, 042413 (2020).
- [91] K. H. Wanser, Fundamental phase noise limit in optical fibres due to temperature fluctuations, *Electronics Letters* **28**, 53 (1992).
- [92] D. Derickson, *Fiber Optic Test and Measurement* (Prentice Hall PTR, New York, 1998).
- [93] B. M. Terhal, Quantum error correction for quantum memories, *Rev. Mod. Phys.* **87**, 307 (2015).
- [94] A. V. Zasedatelev, A. V. Baranikov, D. Sannikov, D. Urbonas, F. Scafrimuto, V. Y. Shishkov, E. S. Andrianov, Y. E. Lozovik, U. Scherf, T. Stöferle, R. F. Mahrt, and P. G. Lagoudakis, Single-photon nonlinearity at room temperature, *Nature* **597**, 493 (2021).
- [95] A. W. Harrow and R. A. Low, Random Quantum Circuits are Approximate 2-designs, *Communications in Mathematical Physics* **291**, 257 (2009).
- [96] C. Dankert, R. Cleve, J. Emerson, and E. Livine, Exact and approximate unitary 2-designs and their application to fidelity estimation, *Phys. Rev. A* **80**, 012304 (2009).
- [97] F. G. S. L. Brandão, A. W. Harrow, and M. Horodecki, Local random quantum circuits are approximate polynomial-designs, *Communications in Mathematical Physics* **346**, 397 (2016).
- [98] J. Haferkamp, Random quantum circuits are approximate unitary, *Quantum* **6**, 795 (2022).
- [99] K. C. Tan, S. Choi, and H. Jeong, Negativity of quasiprobability distributions as a measure of nonclassicality, *Phys. Rev. Lett.* **124**, 110404 (2020).
- [100] C. M. Caves, Quantum limits on noise in linear amplifiers, *Phys. Rev. D* **26**, 1817 (1982).
- [101] C. M. Caves, J. Combes, Z. Jiang, and S. Pandey, Quantum limits on phase-preserving linear amplifiers, *Phys. Rev. A* **86**, 063802 (2012).
- [102] J. J. Guanzon, M. S. Winnel, D. Singh, A. P. Lund, and T. C. Ralph, Saturating the maximum success probability bound for noiseless linear amplification using linear optics, *PRX Quantum* **5**, 020359 (2024).
- [103] J. S. Neergaard-Nielsen, Y. Eto, C.-W. Lee, H. Jeong, and M. Sasaki, Quantum tele-amplification with a continuous-variable superposition state, *Nature Photonics* **7**, 439 (2013).
- [104] J. Fiurášek, Teleportation-based noiseless quantum amplification of coherent states of light, *Opt. Express* **30**, 1466 (2022).
- [105] J. J. Guanzon, M. S. Winnel, A. P. Lund, and T. C. Ralph, Noiseless linear amplification and loss-tolerant quantum relay using coherent-state superpositions, *Phys. Rev. A* **108**, 032411 (2023).
- [106] J. Zhao, H. Jeng, L. O. Conlon, S. Tserkis, B. Shajilal, K. Liu, T. C. Ralph, S. M. Assad, and P. K. Lam, Enhancing quantum teleportation efficacy with noiseless linear amplification, *Nature Communications* **14**, 4745 (2023).
- [107] J. Fiurášek, Analysis of continuous-variable quantum teleportation enhanced by measurement-based noiseless quantum amplification, *Opt. Express* **32**, 2527 (2024).
- [108] I. Jeon, S. Cho, and H. Jeong, *Amplifying hybrid entangled states and superpositions of coherent states* (2024), [arXiv:2409.16562 \[quant-ph\]](https://arxiv.org/abs/2409.16562).
- [109] E. Sendonaris, J. Williams, R. Nehra, R. Gray, R. Sekine, L. Ledezma, and A. Marandi, Ultrafast single-photon detection using nanophotonic parametric amplifiers (2024), [arXiv:2410.18397 \[physics.optics\]](https://arxiv.org/abs/2410.18397).
- [110] M. Reck, A. Zeilinger, H. J. Bernstein, and P. Bertani, Experimental realization of any discrete unitary operator, *Phys. Rev. Lett.* **73**, 58 (1994).
- [111] W. R. Clements, P. C. Humphreys, B. J. Metcalf, W. S. Kolthammer, and I. A. Walmsley, Optimal design for universal multiport interferometers, *Optica* **3**, 1460 (2016).
- [112] C. Arends, L. Wolf, J. Meinecke, S. Barkhofen, T. Weich, and T. J. Bartley, Decomposing large unitaries into multimode devices of arbitrary size, *Phys. Rev. Res.* **6**, L012043 (2024).
- [113] F. Hanamura, W. Asavanant, H. Nagayoshi, A. Sakaguchi, R. Ide, K. Fukui, P. van Loock, and A. Furusawa, Implementing arbitrary multimode continuous-variable quantum gates with fixed non-gaussian states and adaptive linear optics, *Phys. Rev. A* **110**, 022614 (2024).
- [114] T. Hummel, A. Widhalm, J. P. Höpker, K. D. Jöns, J. Chang, A. Fognini, S. Steinhauer, V. Zwiller, A. Zrenner, and T. J. Bartley, Nanosecond gating of superconducting nanowire single-photon detectors using cryogenic bias circuitry, *Opt. Express* **31**, 610 (2023).
- [115] T. Schapeler, N. Lamberty, T. Hummel, F. Schlue, M. Stefszky, B. Brecht, C. Silberhorn, and T. J. Bartley, Electrical trace analysis of superconducting nanowire photon-number-resolving detectors, *Phys. Rev. Appl.* **22**, 014024 (2024).
- [116] B. Collins and P. Śniady, Integration with respect to the Haar measure on unitary, orthogonal and symplectic group, *Communications in Mathematical Physics* **264**, 773 (2006).

- [117] F. Mezzadri, How to generate random matrices from the classical compact groups, *Notices of the AMS* **54**, 592 (2007).
- [118] Z. Puchała and J. Miszczak, Symbolic integration with respect to the Haar measure on the unitary groups, *Bulletin of the Polish Academy of Sciences: Technical Sciences* **65**, 21 (2017).
- [119] A. A. Mele, Introduction to Haar measure tools in quantum information: A beginner's tutorial (2023), [arXiv:2307.08956](https://arxiv.org/abs/2307.08956) [quant-ph].
- [120] T. A. Severini, *Elements of Distribution Theory* (Cambridge University Press, Cambridge, 2005).
- [121] J. Soule, A. C. Doherty, and A. L. Grimsmo, Concatenating binomial codes with the planar code (2024), [arXiv:2312.14390](https://arxiv.org/abs/2312.14390) [quant-ph].
- [122] R. Y. Teh, P. D. Drummond, and M. D. Reid, Overcoming decoherence of Schrödinger cat states formed in a cavity using squeezed-state inputs, *Phys. Rev. Res.* **2**, 043387 (2020).
- [123] D. S. Schlegel, F. Minganti, and V. Savona, Quantum error correction using squeezed Schrödinger cat states, *Phys. Rev. A* **106**, 022431 (2022).
- [124] J. Provazník, P. Marek, J. Laurat, and R. Filip, *Adapting coherent-state superpositions in noisy channels* (2024), [arXiv:2406.01081](https://arxiv.org/abs/2406.01081) [quant-ph].
- [125] B. Royer, S. Singh, and S. M. Girvin, Stabilization of finite-energy Gottesman-Kitaev-Preskill states, *Phys. Rev. Lett.* **125**, 260509 (2020).
- [126] I. Tzitrin, J. E. Bourassa, N. C. Menicucci, and K. K. Sabapathy, Progress towards practical qubit computation using approximate Gottesman-Kitaev-Preskill codes, *Phys. Rev. A* **101**, 032315 (2020).
- [127] I. Rojko, P. M. Röggl, M. Wagener, M. Fontboté-Schmidt, S. Welte, J. Home, and F. Reiter, Two-qubit operations for finite-energy Gottesman-Kitaev-Preskill encodings, *Phys. Rev. Lett.* **133**, 100601 (2024).
- [128] P. Marek, Ground state nature and nonlinear squeezing of Gottesman-Kitaev-Preskill states, *Phys. Rev. Lett.* **132**, 210601 (2024).
- [129] N. Killoran, J. Izaac, N. Quesada, V. Bergholm, M. Amy, and C. Weedbrook, Strawberry fields: A software platform for photonic quantum computing, *Quantum* **3**, 129 (2019).
- [130] T. R. Bromley, J. M. Arrazola, S. Jahangiri, J. Izaac, N. Quesada, A. D. Gran, M. Schuld, J. Swinerton, Z. Zabaneh, and N. Killoran, Applications of near-term photonic quantum computers: software and algorithms, *Quantum Sci. Technol.* **5**, 034010 (2020).
- [131] Y. Yao, F. Miatto, and N. Quesada, Riemannian optimization of photonic quantum circuits in phase and Fock space, *SciPost Physics* **17** (2024).
- [132] T. Hillmann, F. Quijandria, G. Johansson, A. Ferraro, S. Gasparinetti, and G. Ferrini, Universal gate set for continuous-variable quantum computation with microwave circuits, *Phys. Rev. Lett.* **125**, 160501 (2020).
- [133] N. Budinger, A. Furusawa, and P. van Loock, All-optical quantum computing using cubic phase gates, *Phys. Rev. Res.* **6**, 023332 (2024).
- [134] Y. S. Teo, *Introduction to Quantum-State Estimation* (World Scientific, Singapore, 2015).
- [135] J. Peřina, *Quantum Statistics of Linear and Nonlinear Optical Phenomena* (Springer Dordrecht, Dordrecht, 1991).
- [136] A. Serafini, *Quantum Continuous Variables: A Primer of Theoretical Methods* (CRC Press, Boca Raton, 2017).
- [137] K. E. Cahill and R. J. Glauber, Density operators and quasiprobability distributions, *Phys. Rev.* **177**, 1882 (1969).
- [138] J. Řeháček, B.-G. Englert, and D. Kaszlikowski, Minimal qubit tomography, *Phys. Rev. A* **70**, 052321 (2004).
- [139] B. G. Englert, On the operator bases underlying Wigner's, Kirkwood's and Glauber's phase space functions, *Journal of Physics A: Mathematical and General* **22**, 625 (1989).
- [140] S. Boyd and L. Vandenberghe, *Convex Optimization* (Cambridge University Press, Cambridge, 2009).
- [141] M. Grant and S. Boyd, CVX: Matlab software for disciplined convex programming, version 2.1, <http://cvxr.com/cvx> (2014).
- [142] M. Grant and S. Boyd, Graph implementations for nonsmooth convex programs, in *Recent Advances in Learning and Control*, Lecture Notes in Control and Information Sciences, edited by V. Blondel, S. Boyd, and H. Kimura (Springer-Verlag Limited, 2008) pp. 95–110, http://stanford.edu/~boyd/graph_dcp.html.
- [143] S. Izumi, M. Takeoka, K. Wakui, M. Fujiwara, K. Ema, and M. Sasaki, Projective measurement onto arbitrary superposition of weak coherent state bases, *Scientific Reports* **8**, 2999 (2018).
- [144] Z. Holmes, K. Sharma, M. Cerezo, and P. J. Coles, Connecting ansatz expressibility to gradient magnitudes and barren plateaus, *PRX Quantum* **3**, 010313 (2022).
- [145] Y. S. Teo, S. Shin, H. Kwon, S.-H. Lee, and H. Jeong, Virtual distillation with noise dilution, *Phys. Rev. A* **107**, 022608 (2023).